Dissertations, Theses, and Masters Projects   Theses, Dissertations, & Master Projects

1963

On the Problem of Radio Signal Attenuation during Hypervelocity Reentry

David Joseph Romeo
College of William & Mary - Arts & Sciences

ON THE PROBLEM OF RADIO SIGNAL ATTENUATION

DURING HYPERVELOCITY REENTRY

———————

A Thesis

Presented to

The Faculty of the Department of Physics

The College of William and Mary in Virginia

———————

In Partial Fulfillment

Of the Requirements for the Degree of

Master of Arts

———————

David Joseph Romeo

August 1963

ON THE PROBLEM OF RADIO SIGNAL ATTENUATION

DURING HYPERVELOCITY REENTRY

———————

A Thesis

Presented to

The Faculty of the Department of Physics

The College of William and Mary in Virginia

———————

In Partial Fulfillment

Of the Requirements for the Degree of

Master of Arts

———————

David Joseph Romeo

August 1963

ACKNOWLEDGMENTS

iii

TABLE OF CONTENTS

LIST OF FIGURES

ABSTRACT

The problem of radio signal attenuation during hypervelocity reentry is reviewed and application of the forward facing jet to this problem is considered. The effect on the bow shock of a blunt body caused by the forward facing jet was investigated experimentally at NASA Langley Research Center facilities and data from the published report of theat investigation is considered here with a view toward application of the results to the radio attenuation problem.

ON THE PROBLEM OF RADIO SIGNAL ATTENUATION

DURING HYPERVELOCITY REENTRY

INTRODUCTION

At the present time a problem that is of great concern to the safe
recovery of hypervelocity space vehicles lies in maintaining continuous
data transmission and communication contact between the vehicle and the
ground during the critical braking period of the reentry maneuver. Con-
tinuous radio transmission is, at the present time, lost during this period
due to the strong bow shock that forms around the body. The temperature
through this shock is raised enough to ionize the gas in front of the
vehicle which in turn prevents transmission of the signal. That is,
the ionized gas layer, or plasma, has a finite electrical conductivity
which may absorb and, or reflect the radio signal. Several solutions to
this problem are at the present time under consideration and are being
examined experimentally.

One method which has shown some success, does not attempt to alter
the plasma but rather relies on the use of very high frequency signals
which are not attenuated by the ionized gas layer. This approach while
basically simple in concept unfortunately brings about many new problems
involving equipment development. In addition, at certain high frequencies
atmosphere attenuation has to be contended with. Since the necessary
transmission and reception gear are not available for wide application of
this method at the present time, it is worthwhile to look at other
solutions. Existing electronic equipment could, of course, be used if it
were possible to decrease the amount of ionization behind the vehicle bow

2

shock to a degree that would allow satisfactory transmission. Liquid injection methods which cool the plasma and thereby induce recombination have been considered and show some promise of success. Another method, namely, the use of an injected gas, has been given little consideration up until now because of its increased complexity compared to a liquid and because, no advantage of employing of a gas over a liquid has been adequately shown. The present discussion given in this paper will help to demonstrate a marked advantage that an injected gas can have over a liquid. This advantage lies in the ability of the gas in certain instances (referred to in the text as large shock displacements) to alter greatly the shape and the local strength of the main stream shock, thereby not only lessening the degree of ionization by cooling as a liquid does, but by decreasing the extent of the plasma altogether.

The present paper includes information for the prediction of these large shock displacements and in addition provides a possible theoretical explanation for the occurrence of them. An understanding of this phenomenon thus permits consideration to be given to a gas injection device as a way to help alleviate the radio attenuation problem. Although general consideration here is given to the application of the injected gas method for relieving radio attenuation it was not possible to explore many experimental phases of the problem. The majority of the experimental and theoretical work considered here is concentrated on showing the flow phenomena and establishing the criteria that would enable a forward-facing jet to be used as a means of increasing the possibility of radio transmission through the bow shock.

LIST OF SYMBOLS

d_j — jet-exit diameter

d_m — model diameter at jet exit

E — electric field vector

$\tilde{e}$ — electron charge

f_c — collision frequency

f_p — plasma frequency

f_s — frequency of signal

J — current density

K — attenuation

l — distance; between the foremost point of the main stream shock and the model face, measured along the model center line

l_1 — distance between the initial intersection of the jet mixing region and the model face measured along the model center line

M — Mach number

m_e — electron mass

N_e — electron concentration

n — phase constant

n_0 — Loschmidts number (2.686×10^{19} cm^{-3})

p	pressure
t	temperature
V	velocity
X_e	electron mole portion
α	angle of attack measured between main stream flow direction and model center line
γ	ratio of specific heats
ϵ	permittivity of free space
θ	oblique shock angle
μ	permeability
ν	angle through which flow must expand from $M = 1.0$ to a given Mach number
σ	scalar electrical conductivity

Subscripts:

o	standard or initial conditions (for pressure 1 atm, for temperature, ice point)
∞	free-stream, test-section conditions
j	jet free-stream conditions at exit, nominal value
t	stagnation condition
max	maximum
1.	condition at jet nozzle just inside exit
2.	condition at jet nozzle just outside exit

A prime mark denotes condition after a normal shock.

CHAPTER I

THE BLACKOUT PROBLEM

As a blunt body reenters the earth's atmosphere at a high velocity the air in front of the body is forced to pass through a large pressure discontinuity or bow shock. It is by virtue of this shock that the kinetic energy of the vehicle is converted to heat as the body decelerates. This method of vehicle deceleration is responsible for the existence of extremely high temperature gases in the vicinity of the body. As the temperature increases the oxygen and nitrogen molecules in the gas behind the bow shock dissociate and lead to the release of free electrons. The reactions leading to the release of these electrons can be thought of briefly as follows. In crossing the bow shock, the air moleucles undergo a large number of collisions. Part of the kinetic energy of the vehicle is absorbed as these collisions raise the temperature of the gas to a maximum value. Further collisions cause the air molecules to dissociate. The single atoms may then recombine in a manner in which free electrons are released, for example, monatomic nitrogen and oxygen recombining release an electron, $N + O \rightarrow NO^+ + e^-$. Other chemical reactions also result in the direct ionization of the atomic particles, for example, $N \rightarrow N^+ + e^-$. Descriptions of this phenomena are common and may be readily found in the literature. Reference 1, for example, presents charts relating the thermodynamic properties for air in chemical

6

equilibrium for temperatures up to 15,000° K and for pressure from
10^{-5} to 10^{4} atmospheres. As a direct result of this phenomena a high
concentration of free electrons exists behind the shock and it is the
presence of these free electrons which causes the attenuation of radio
signals. Since the electron concentration of the plasma is a function
of the state properties of the gas, the density of the free electrons
(that is, electron concentration per cubic centimeter, N_e), can be
calculated if the flow field associated with the plasma is defined.
Briefly, $N_e = X_e n_0 \dfrac{p'_{t,\infty}/p_o}{T'_{t,\infty}/T_o}$. That is, N_e is equal to the product of
the electron mole fraction X_e, Loschmidts number, N_o, and the ratio of
pressure behind the bow shock to sea-level pressure divided by temperature
behind the bow shock to ice point temperature. Reference 2, which makes
use of hypersonic vehicle data over a range of flight velocities and
altitudes, presents computed electron concentrations existing behind the
bow shock of the vehicle and these results are shown in figures 1 and 2.
Figure 1 is a plot of the pressure and temperature existing behind the
bow shock of a reentering body as a function of vehicle velocity.
Included is the altitude at which these pressures exist. From this
figure, and from the altitude versus density relation it is possible to
calculate the electron concentration behind the bow shock; this is shown
in figure 2. Once the electron concentration is known as a function of
altitude, for example, it is possible to obtain an estimate of the amount
of radio signal attenuation caused by N_e. Before proceeding with this,
however, it is necessary to introduce one more flow criterion. In the
above curves it has been assumed that the plasma has had sufficient time

to reach equilibrium conditions. For the case of normal shock waves at high Mach numbers this is a good assumption since it has been shown (ref. 3, for example) that the distance needed behind the shock to reach these conditions is quite small. Figure 3, taken from reference 3, shows data obtained in a low density shock tube which illustrates that the ionization distance for chemical equilibrium in air is of the order of a few centimeters for the free-stream Mach numbers encountered during reentry. In addition it can be seen that the ionization distance decreases as the free-stream Mach number increases. Included on the figure is a curve representing the theory of Lin and Teare, reference 4. This assumption of complete equilibrium is on the conservative side because of a lack of complete equilibrium would mean lower electron concentrations and less signal attenuation. Associated with the electron concentration N_e, is the plasma frequency, f_p, and this quantity is also shown in figure 2. The plasma frequency is a parameter proportional to the square root of free electron concentration in the plasma and is a measure of the natural oscillation of an average free electron (for an infinite plasma). For example, in a plasma in which some of the electrons have been displaced from their equilibrium position by an external force, a restoring field is created which, if the force is removed, will cause the electrons to oscillate about their equilibrium position. A second important property of the plasma is the electron collision frequency. This parameter is equal to the average number of collisions undergone by each particle per unit time. (See ref. 5, for example.) These two characteristics are responsible for attenuation of a radio signal passing

through the plasma. To determine a quantitative approximation of the amount of signal reduction caused by a given plasma, the following theory based primarily on the theories given in references 5 and 7, is given. Certain simplifying assumptions will first be made which enable solutions but do not, as will be seen later, alter seriously the results. The electromagnetic theory briefly presented is for plane wave, monocromatic radiation interacting with a plane homogeneous semi-infinite medium in thermodynamic equilibrium.

Consider a plane wave normally incident upon a semi-infinite uniform plasma. The boundary is a discontinuous jump from free space values to the plasma values. At the boundary, part of the wave may be reflected and the rest transmitted into the plasma. Figure 4 taken from reference 8 qualitatively illustrates this phenomenon for two plasma conditions. In case 4(a) the plasma frequency is approximately equal to the plasma collision frequency. It can be seen that the cutoff for reflection and absorption is quite gradual; in the second case 4(b) ($f_p \gg f_c$) the cutoff is very sharp, and when the signal frequency is well below f_p almost the entire wave is reflected. Since the second case corresponds to plasma conditions at the beginning of reentry (fig. 5 taken from ref. 9) if the signal frequency is small practically no propagation through the plasma could even be expected. It is necessary, therefore, to have a signal frequency near or greater than the plasma frequency if transmission is to be attained. For this reason high signal frequencies are used and the problem of first importance becomes one of absorption rather than reflection. For this reason only the transmitted part of the wave will be considered in this paper.

To proceed with the theory it can be said that if the signal wave length in the plasma is much greater than the electron mean free path of the plasma, the ionized gas can be assumed to be an uncharged conducting continuum. (See ref. 6.) The wave equation for this medium is (for example, ref. 10)

$$\nabla^2 E - \mu\epsilon \frac{\partial^2 E}{\partial t^2} - \mu\sigma \frac{\partial E}{\partial t} = 0 \tag{1}$$

and for a wave traveling in the x direction

$$\frac{\partial^2 E}{\partial x^2} - \mu\epsilon \frac{\partial^2 E}{\partial t^2} - \mu\sigma \frac{\partial E}{\partial t} = 0 \tag{2}$$

Assuming a harmonic solution for this equation results in

$$E = E_0 e^{2\pi j\, f_s t - jnx - Kx}$$

where

$$(K + jn)^2 = -\mu\epsilon(2\pi f_s)^2 + j\mu\sigma(2\pi f_s) \tag{3}$$

K is the attenuation constant and n is the phase constant.

Next consider an electron in motion in a periodic electric field which is polarized in the y direction, the field can be represented as

$$E = E_0 e^{2\pi j f_s t} \tag{4}$$

Writing the equation of motion of the particle, including a damping force due to electron collision gives

$$m_e \frac{d^2y}{dt^2} = \tilde{e}E - 2\pi f_c m_e \frac{dy}{dt} \tag{5}$$

where $\tilde{e}$ is the electron charge. Substituting equation (4) and rewriting

$$m_e \frac{d^2y}{dt^2} + 2\pi f_c m_e \frac{dy}{dt} = \tilde{e}E_o e^{2\pi j f_s t} \tag{6}$$

Assuming the plasma electron collision frequency, f_c, to be a constant allows the solution

$$y = \frac{1}{(2\pi f_c + 2\pi j f_s)} \frac{j\tilde{e}}{(2\pi f_s m_e)} E_o e^{2\pi j f_s t} \tag{7}$$

The current density associated with the moving electrons is (ref. 6)

$$J = N_e \tilde{e} \frac{dy}{dt} \tag{8}$$

$\frac{dy}{dt}$ is again the electron velocity. Substitution of the velocity term using the first derivative of equation (7) yields

$$J = \frac{N_e \tilde{e}^2}{(2\pi f_c + 2\pi j f_s)} \frac{E}{m_e} \tag{9}$$

Using Ohms law $J = \sigma E$ and substituting into equation (9)

$$\sigma = N_e \frac{\tilde{e}^2}{m_e} \frac{1}{(2\pi f_c + 2\pi j f_s)} \tag{10}$$

and substitution of equation (10) back into equation (3(a)) for the attenuation constant gives (see again, refs. 5 through 7)

$$K = \frac{2\pi f_s}{c}\left\{\frac{1}{2}\left(1 - \frac{f_p^2}{f_c^2 + f_s^2}\right)\left[-1 + \sqrt{1 + \left\{\frac{f_p^2 f_c}{f_s\left(1 - \dfrac{f_p^2}{f_c^2 + f_s^2}\right)\left(f_c^2 + f_s^2\right)}\right\}^2}\right]\right\}^{\frac{1}{2}}$$

(11)

for the attenuation coefficient.

Solutions to the plane wave equations for the transmitted portion of the signal are presented in figure 6, reference 2. It can be seen that for values of plasma frequency much larger than the collision frequency, $f_p \gg f_c$ the signal will be cut off sharply for values of f_s approximately equal to f_p. For values of $f_p \approx f_c$, however, the attenuation is much more gradual. The range of $f_p \gg f_c$ is associated with high altitudes and values of $f_p \approx f_c$ are associated with low altitudes. If f_s is less than the maximum value of f_p, therefore, the signal would be cut off sharply as reentry begins and the return of the signal at lower altitudes (as f_p again is reduced to f_s) would be gradual and difficult to predict. To compare this prediction with actual flight test data consider figure 7. Here on a plasma frequency-velocity plot is shown the MA-6 Mercury flight reentry trajectory (ref. 8). From the theory one would expect significant attenuation of C-band telemetry (5.5 KMC) for the part of the trajectory above a line drawn at a plasma frequency value of 5.5 KMC. Actual attenuation of C-band telemetry did indeed occur during reentry but not for as great a part of the trajectory as indicated by the simple theory. It is seen from the figure, however,

that the theory has predicted an inclusive envelope in which radio blackout did occur.

Attenuation of other signal frequencies may be approximated in the same manner as was done for the C-band signal. At certain frequencies above C-band; however, atmospheric attenuation becomes a problem which must also be given consideration. Figure 8, taken from reference 11, for example, illustrates how atmospheric attenuation enters the problem at signal frequencies much above 10 KMC. The plasma conditions given in figure 7 are those existing at the most severe part of the flow (that is, behind a normal shock) but since other positions in the plasma are so dependent on local flow conditions which depend for example, on vehicle shape, flow separation, and so forth, they were not considered for the blunt body case.

The signal blackout problem has been established and it remains now to show that the jet probe proposal can be applied to this problem and that some degree of success of the proposed method can be established.

CHAPTER II

RESULTS OF WORK DONE ON THE JET PROBE

The expression "jet probe" or "forward-facing jet" as used in
this paper refers to the concept of a gas jet issuing directly forward
from a high-speed blunt body. The jet alters the strength and shape
of the bow shock of the body, from which it is flowing and thereby
has a large influence on the aerodynamic characteristics of the body.

Before considering the application of the jet probe to the black-
out problem, it is desirable to look into the fluid flow studies that
have been done on the jet both experimentally and theoretically. A
review of this work is a necessary part of understanding the reasons
why little consideration has been given to the jet in work done on the
blackout problem thus far. Regions of exploration of this concept are
given and present limitations of the use of the probe are pointed out.

The idea of injecting a gas forward into a free-stream flow was
explored as early as 1951 when some investigations were made (ref. 12)
to determine the effect of a sonic jet on the drag of a blunt body
in transonic flow. It was observed in that paper (also subsequently
in refs. 13-17) that the jet issuing upstream at a high exhaust velocity
could cause a large change in the aerodynamic characteristics of the
body from which it was emerging. This work was extended by the author

14

and Mr. J. R. Sterrett at a free-stream Mach number of 6.0 with additional interesting results (ref. 18), which are now given.

High-speed movies showed that the alteration of the main-stream shock caused by a forward-facing jet can be placed into two distinct categories. In one case the jet produces no apparent change in the bow shock over the body other than to cause it to increase in size. In other words, the main-stream flow appears to see an increasingly larger blunt body as the jet pressure is increased. The bow shock in this case is quite steady and the flow phenomena is similar to that normally observed with gas or liquid injection (for example, refs. 12-17). In the second case, an effect which was quite different was observed; the main-stream shock was far removed from the face of the model. It is in this condition that the jet may have the ability to permit successful radio transmission. An excellent illustration of the two cases of shock displacement can be seen in figure 9 for a model which has a nominal jet-exit Mach number of 6.4 and a ratio of model diameter to jet-exit diameter (d_m/d_j) of 1.12. The photos for a ratio of jet-total pressure to free-stream total pressure $(p_{t,j}/p_{t,\infty})$ of 1.14 through 2.51 show that the main-stream shock for this range is essentially of the same shape as a bow shock over a blunt body with no jet flow; this, therefore, is an example of the first case mentioned above. These photos also show that the jet itself has gone through a normal or overexpansion shock before meeting the main stream. Merely as a means of convenience this effect on the main-stream shock will be referred to as the strong case, referring to the bow type main-stream

shock and the strong overexpansion shock in the jet. The second case, the case of large main-stream shock displacements, is seen in the photos for variations in $p_{t,j}/p_{t,\infty}$ from 0.45 through 0.86. Here, as stated above, the main-stream shock is far removed from the face of the model, as much as eight times that for the case of the strong shock. The example shown in figure 9 is for a model in which air was used as the jet gas. The effect of the use of helium as the jet gas may be found in figure 10.

The graphical determination of the main-stream displacement distances for the examples for figures 9 and 10 are shown in figures 11 and 12. These data show the measured shock displacement distance divided by model diameter plotted versus jet-to-free-stream total-pressure ratio.

While figures 9-12 are examples of the data obtained in the experiments of reference 18 for particular models, figures 13 and 14 are summary plots of these data. Figure 13 shows maximum values of l/d_m (the ratio of shock stand-off distance to model diameter) plotted versus model angle of attack. A rapid decrease is seen in l_{max}/d_m as the angle of attack is increased even slightly. Figure 14 is a plot of l/d_m as nominal exit Mach number for the tests in which a maximum appeared to have been reached. It can be seen here that l_{max}/d_m increases greatly with jet exit Mach number for all the models tested. The plot also illustrates the decrease in l_{max}/d_m for any given Mach number as d_m/d_j increases. Since the data for this plot were taken from both the air and the helium tests the Mach number variation tends to ignore other differences in the properties of the gases on l_{max}/d_m. It cannot be said here that the jet exit Mach number plays

the only role in the marked increased in l_{max}/d_m when helium instead of air was tested in models, but this question will be given further consideration.

Summarizing the experimental results of reference 18 we find that in general:

1. The nature of the alteration of the main-stream shock caused by the jet could be placed into two distinct categories. In one case, the bow shock was forced away from the body but retained its basic shape. In the second case the shock was far removed from the body and appeared to be less steady than in the first case.

2. The case when the large displacements were observed was seen to occur at higher values of total pressure ratio either as the jet exit Mach number of the model to jet-exit-diameter ratio was increased.

3. When the large displacement case occurred, the length of the displacement with respect to model diameter was seen to increase as the jet exit Mach number was increased from 1 to 10.3, and also as the model to jet-exit-diameter ratio was decreased and approached 1.0.

4. The large displacement of the main-stream shock was observed to fall off rapidly as the angle of attack was increased.

CHAPTER III

THEORETICAL DISCUSSION OF THE JET PROBE FLOW FIELD

The most significant result of the experimental data reviewed in
chapter II was the observation of a large displacement of the bow shock
under certain test conditions. These conditions had not been previously
defined in terms of jet pressure, jet Mach number, etc.

Because of the importance of the large displacement phenomenon
in the application of the jet probe to the blackout problem; and
because this phenomenon is new, it is felt that an inclusion of a
possible qualitative explanation of the concept should be presented.
Perhaps a good place to start would be with an explanation of what the
jet flow does as it exhausts from the exit of the probe.

A jet exhausting into still air or into an opposing stream will
expand if the pressure just outside the jet is less than the pressure
in the jet at the exit, that is, if $p_1/p_2 > 1$. (See fig. 15.) If the
pressure just outside is greater $(p_1/p_2 < 1)$ the jet will compress. In
addition if the jet flow at the exit is sonic or supersonic that is,
if $M_j \geq 1$, expansion waves will form at the exit for the case where the
jet flow expands and compression waves will form for the case where jet
flow is forced to compress. In either case these waves will cross the
exhausting jet and will be reflected at the jet boundaries. (See
figs. 15(a) and (b) and 19 and 20.) Associated with the jet flow are

18

regions of mixing in the boundaries of the jet and the outside flow.
No data are at present available which give the thickness of this
mixing region for two opposing flows or two flows at high Mach numbers.
References 21 and 22, however, present data which show that for a jet
exhausting at low supersonic Mach numbers into quiescent air the region
of mixing will extend approximately 3° to either side of the theoretical
jet boundary. Due to the absence of data at other Mach numbers this 3°
mixing region was assumed for all cases in this study. One result of
reference 22 was that the mixing region was not influenced significantly
by the jet exit Mach number for the range tested. Before proceeding to
a method for predicting theoretically under what conditions the jet
exhausting from the body will enter into the strong shock case or the
large displacement case noted in the experimental results, and sketched
for reference in figures 15(a) and (b), one more flow condition must be
established. As the flows on the center line of the jet and the main
supersonic opposing flow come to a mutual stagnation point with respect
to the probe (fig. 15), as they must, the stagnation pressures of both
flows must be equal. This requirement is perhaps the most significant
one associated with the whole flow phenomenon because it is believed to
be the condition which determines the behavior of the supersonic jet
flow. At the stagnation point, therefore,

$$p'_{t,j} = p'_{t,\infty} \qquad (1)$$

or

$$\frac{p'_{t,j}}{p_{t,j}} = \frac{p'_{t,\infty}}{p_{t,\infty}} \frac{p_{t,\infty}}{p_{t,j}} \qquad (1(a))$$

where a prime denotes conditions after a normal shock. For a given supersonic main stream Mach number $\frac{p'_{t,\infty}}{p_{t,\infty}}$ is fixed (for example, ref. 23). For a given ratio of main stream to jet total pressure $\frac{p_{t,\infty}}{p_{t,j}}$, therefore it is seen that $\frac{p'_{t,j}}{p_{t,j}}$ is fixed (eq. (1(a)) which means the supersonic Mach number at which the jet overexpands or goes through a normal shock, is also fixed. For example, consider a jet exhausting at a given Mach number and a main stream flow at an identical Mach number. If the jet and main stream total pressure are equal, $\frac{p_{t,j}}{p_{t,\infty}} = 1$, then a normal shock will occur just at the jet exit and a stagnation point will occur very close to the jet exit similar to figure 15(a). If, however, $\frac{p_{t,j}}{p_{t,\infty}} > 1$ the jet must expand (that is, the gas accelerates to a higher Mach number) as it leaves the nozzle in order to satisfy inviscid normal shock relations (eq. 1(a)). Up to now the existing pressure ratio p_1/p_2 for this case (fig. 15) has not been considered, but it was pointed out that if $p_1/p_2 < 1$ the jet would compress and slow down as it leaves the nozzle. Conceivable it could occur, due to exterior boundary conditions that $\frac{p_{t,j}}{p_{t,\infty}} > 1$ requiring an expansion for normal shock restrictions and $p_1/p_2 < 1$ requiring a compression. Since these two conditions cannot, of course, simultaneously occur it must be reasoned that if $p_1/p_2 < 1$ inviscid normal shock conditions are not satisfied. In other words the jet cannot directly go through a normal shock in order to satisfy $p'_{t,j} = p'_{t,\infty}$. This incompatibility can be removed, however, by considering the jet mixing region, since a loss in total head through the mixing region could allow all above conditions to be met. That is, if the jet cannot expand sufficiently to meet both exit and center-line

stagnation pressure conditions, then some viscous mixing evidently must take place along the center line to account for the necessary jet pressure reduction. (See fig. 15(b).) Qualitatively, then the conditions of strong shock case (fig. 15(a)) and large displacement case (fig. 15(b)) have been given an explanation. Next some quantitative examples of the two cases will be given. These examples are for a jet exhausting into still air and are therefore much easier to handle than the two flow problems. However, they still give results which are believed to be analogous to the actual two opposing flow problems.

Coarse net characteristic diagrams for two-dimensional jets exhausting into still air at several values of p_1/p_2 are sketched in figure 16. The pressure ratio ($p_2/p_\infty = 1.3$) was held constant and the total pressure of the jet was varied to produce different values of p_1/p_2. That is

$$\frac{p_1}{p_2} = \frac{p_\infty}{p_2} \frac{p_{t,j}}{p_{t,\infty}} \frac{p_1}{p_{t,j}} \frac{p_{t,\infty}}{p_\infty} \tag{2}$$

where the first term on the right is held constant, the second term is varied and the third and fourth terms are fixed for a given jet model and free-stream Mach number. Also shown in figure 16 are the assumed 3° mixing regions. These four sketches illustrate the conditions for the large displacement type and the strong shock type of flow occurrence. In figure 16(a) it can be seen that $p'_{t,j} > p'_{t,\infty}$ everywhere on the center line before mixing occurs and, therefore, for equal stagnation pressures (a condition that must be met somewhere on the center line) some mixing

must take place to decrease the total pressure of the jet. In this
figure and also in figures 16(b) and 16(c) the jet cannot expand to a
Mach number high enough for $p'_{t,j}$ to be equal to $p'_{t,\infty}$ without mixing
energy loss because of the exit-pressure ratio p_1/p_2. These cases
where mixing occurs are believed to be the cases where the large displace-
ment type patterns occurred in the experimental data, and are of the type
sketched in figure 15(b). When the conditions are such that mixing must
take place, the distance the jet penetrates into the main stream is
much greater than a case where a mixing loss is not required to satisfy
center-line conditions. A case where $p_{t,j}/p_{t,\infty}$ is large enough to
allow an expansion and normal shock loss sufficient to satisfy center-
line conditions without a mixing loss is shown in figure 16(d), and
this case is similar to the one sketched in figure 15(a). Here the distance
to the normal shock is much less than in the above cases and this is an
example of the strong shock case. Now that two different types of flow
conditions have been discussed for the simple two-dimensional model
exhausting into still air and these two different types have been associated
with what has been experimentally observed, it is interesting to look
next at the regions at which these two different types occur and to see
how these regions vary theoretically. Figure 17 for different jet-exit
Mach numbers shows these regions. The solid line on the figure represents
the Mach number necessary for $p'_{t,j}$ to equal $p'_{t,\infty}$, and is obtained
from equation 1(a) for $M_\infty = 6.00$. The dashed lines are the maximum jet
Mach numbers that can be reached on the center line by expansion from
the jet exit and are obtained from equation (2) and from

$$v_{max} = v_1 + 2(v_2 - v_1) \tag{3}$$

where v is the Prandtl-Meyer expansion angle, or angle through which a sonic flow must turn in order to expand to a given Mach number.

Flow conditions representing the strong shock case would occur above the intersection of the dashed and solid lines and large displacement cases would occur below the intersection. The maximum $p_{t,j}/p_{t,\infty}$ for large displacement at any given Mach number increases as the exit-pressure ratio p_2/p_∞ increases. This agrees with the experimental data if it is assumed that increasing the body-to-jet-exit-diameter ratio increases p_2/p_∞. Also seen is the fact that the jet-exit Mach numbers are very important in that the maximum values of $p_{t,j}/p_{t,\infty}$ for large displacement increase rapidly as the exit Mach number increases. This same trend of increasing maximum $p_{t,j}/p_{t,\infty}$ with increasing exit Mach number was exactly what was observed experimentally. For low, nearly sonic exit Mach numbers the region over which large displacements occur is very short. Because of this and because other investigations up until now have not been run at high exit Mach numbers these phenomena of large displacements have not received much attention as was mentioned in chapter I. Figure 18 is a replot of figure 17 except that helium was used as the jet gas. These curves are similar in trend but the most important thing to see here is that the maximum values of $p_{t,j}/p_{t,\infty}$ for large type displacements for a given p_2/p_∞ is very much greater for helium than for air. This again was noted experimentally.

Theoretical examples based on two-dimensional flow into still air have thus been given which help to explain the observed experimental results of the more complicated, two opposing flow problems.

CHAPTER IV

APPLICATION OF THE JET PROBE TO THE BLACKOUT PROBLEM

The results of the experimental tests reviewed in chapter II have shown that the forward facing jet can cause a large alteration of the bow shock of a blunt body. In order to apply these results to a typical ballistic reentry body for which the blackout problem was defined in chapter I refer first to the sketch of figure 19. Here the blunt body is used as an antenna probe extending through but not altering the main bow shock. To use the jet to alter the parent bow shock will not be considered because it must be assumed that the method used to allow radio transmission will not alter to any significant degree the aerodynamic characteristics of the parent vehicle. A small probe of this type would be subject to heating along the sides of the probe but it will be assumed that the jet flow will be sufficient to cool the probe adequately in this region and that the face of the probe which is subjected to the normal part of the bow shock will also have sufficient protection when the gas is being used. A small probe without cooling could not survive the reentry heat. The blunt probe will have a strong bow-type shock associated with it and will have initial electron concentrations and plasma frequencies identical to the level behind the bow shock of the blunt parent vehicle (assuming equilibrium distance is very small). These conditions have already

been discussed in chapter I. Thus the ionization problem associated
with the blunt antenna probe will be nearly identical to that of the
parent vehicle. For this discussion the gas jet operating at a strong
shock condition will not be considered. It is true that the strong
shock case for the jet (similar to liquid injection), is itself a means of
reducing the amount of electron concentration at the probe, but in this
discussion it is desired to show the increased ability given by the jet when
operated so as to establish the case of large displacements. Data actually
needed in accurately computing the degree of electron concentration at
the face of the antenna, such as how the two flows mix, recombination
times, face and flow temperatures, and so forth, have not been obtained
experimentally. Factors which may be approximated from the results of
reference 18, however, such an antenna face pressure and geometric area
ratios, suggest that the jet may be used successfully and by making
further assumptions a model case will be considered. From the experi-
mental results (chapter II) the design parameters for the jet can be
established (such as $d_m/d_j = 1$, high jet exit Mach number, and so forth).
It will be assumed that with these data it is technically possible to
design a jet antenna which will operate at the condition of large dis-
placements throughout the part of the reentry maneuver where attenuation
reduction is needed.

It has been shown that the jet, when operating in the large dis-
placement region, mixes with the free-stream flow far ahead of the body.
(See fig. 20(c).) Furthermore, the air that goes through the strongest
part of the bow shock must, in addition to mixing, expand rapidly around

the probe. The distance the main stream gas behind the bow shock must travel while mixing with the jet gas will provide time for cooling, and some recombination. The distance traveled, and the amount of mixing, is large when compared to the relatively short stand-off distance of the strong shock case, figure 20(b). In addition, the schlieren photographs show that the size of the normal or strong part of the bow shock is decreased and the shock wave in the proximity of the antenna face is relatively oblique. Free-stream air crossing an oblique shock wave will encounter a much smaller rise in temperature than it would in crossing a normal shock. A few measurements of the oblique shock angle at the axial position of the jet probe face were made from the schlieren photographs and these data are shown in figure 21. It is seen that this angle is relatively independent of the jet parameters as long as the jet is operating in the large displacements regime. More important, however, is the fact that this angle is only slightly larger than the free-stream Mach wave angle (a compression wave caused by an infinitely small disturbance). Since the Mach angle decreases rapidly with increasing free-stream Mach number, figure 21, it is encouraging to see that the flow has nearly expanded to these conditions, because it suggests that the shock angle at the probe may be even less at free-stream Mach numbers higher than that tested. Since the less normal is the shock wave angle, the less will be the resulting electron concentration and the lower will be the plasma frequency, it is, of course, desirable to look for partial alleviation of the blackout problem along these lines. By assuming equilibrium conditions to exist directly behind the shock (a situation much more severe than actually occurs, as will be seen below)

it is possible to calculate the plasma frequency behind the oblique
shock and compare it to the more severe normal shock case. The plasma
conditions existing behind the oblique part of the shock have been
approximated as a function of shock angle in the following manner.
The state properties existing behind an oblique shock with a shock
angle θ at a free-stream Mach number M_1 are identical to the
properties existing behind a normal shock wave occurring at a free-
stream Mach number of M_2, where $M_2 = M_1 \sin \theta$. This is due to the
fact that an oblique shock wave acts as a normal shock to the flow
perpendicular to it. (See, for example, ref. 24.) At a given altitude,
therefore, since the local free-stream speed of sound is the same for
both cases, the velocities of the two cases are related in the same
manner, $V_2 = V_1 \sin \theta$. As a function of θ, therefore, plasma frequencies
were found by tracing along constant altitude lines in figure 7 to the
calculated V_2 and reading the value of plasma frequency on the ordinate.
For the Mercury trajectory shown in figure 7 the plasma frequencies f_p
have been obtained using this method and these results along with the
normal shock case are shown in figure 22. This figure shows that the
maximum plasma frequency obtained in the trajectory shown decreases as
the shock angle decreases. An angle of 50° for example, has reduced
the maximum plasma frequency by almost a half an order of magnitude
over the normal shock value. In the above calculations chemical
equilibrium was assumed to exist immediately behind the flow. Actually
the equilibrium distances for the outer portions that is the oblique
part of the shock wave are finite. (See ref. 3.) In addition, the

expansion of the flow in this region will help to reduce the degree of ionization. Figures 23 and 24 are sketches from unpublished calculations which show the ionization distance, and percent of ionization to equilibrium ionization as functions of oblique shock angle. Figure 23 shows an increase in ionization distance of almost two orders of magnitude as a normal shock is reduced to an oblique angle of around 20°. Figure 24 shows that reducing the bow shock angle decreases the percent of concentration that will reach equilibrium conditions. In addition, the gas used in the jet, can be selected, as one with a large affinity for electrons. Reference 25, for example, has shown that water vapor has the ability to reduce significantly electron concentrations in rocket exhausts. Finally from what has been determined experimentally and theoretically the pressures at the front of the probe are known to be very much lower than the stagnation pressure behind the normal part of the shock. With the assumption that the pressure on the face of the probe is 1.25 p_∞ (based on correlation between theory and data of ref. 18) a second curve labeled probe has been drawn for comparison in figure 7. This reduction pressure at the face of the antenna again accounts for a reduction in maximum plasma frequency reached. The value is an order of magnitude lower than the blunt face bow shock values (MA-6 flight).

Despite these encouraging trends a disadvantage of the jet system exists which needs further consideration. This disadvantage of the jet system is the instability in the occurrence of the large displacement phenomenon at even small angles of attack. This occurrence of instability

has already been noted in chapter II. A small flow misalinement
evidently disrupts the boundary pressures at the jet allowing the jet
flow to overexpand and shorten the penetration distance. (See fig. 13.)
An occurrence of the loss of large displacements with even small
angle of attack would result in a loss of most of the advantages listed
above. At the present time it cannot be said whether this instability
problem can be resolved easily with additional aerodynamic design or
whether it will continue to be a serious drawback, despite further
investigation.

Summarizing the benefits of the jet probe we find that a reduction
in plasma frequency has been shown to exist at the probe for the following
reasons:

1. The size of the normal part of the bow shock was reduced.

2. The bow shock was forced to occur far ahead of the probe, thus
allowing an increase in time and distance for cooling by mixing, and
recombination.

3. The air that crosses the oblique part of the shock receives
much less thermal agitation and, therefore, has a lower plasma fre-
quency than the normal portion of the shock.

4. The equilibrium distance for the oblique shock is finite, that
is, not zero.

5. The pressures existing in the proximity of the face are much
lower than the stagnation pressure existing behind the bow shock.

6. A gas with a large affinity for electrons can be selected for
use with the probe.

Most of the assumptions made at the present time in the calculation which indicated the successful use of a forward facing jet need to be verified experimentally before it can finally be said that the jet will be as successful as proposed. Particular interest is directed to the field of the investigation of the actual electron concentration history through the distance the plasma must travel from the shock to the face of the probe. In addition, much more has to be known about the jet plasma mixing process, and tests need to be run using gases with high absorption cross sections. All of these areas of interest are so complex that in the end actual free-flight test models with all variables represented will probably need to be tested. All of these areas of interest must be considered before successful operation of the jet probe can be predicted. Consideration of these problems has become worthwhile, however, in view of the experimental results treated here which have given indication that the forward facing jet may have useful application in helping to solve the blackout problem.

CHAPTER V

CONCLUDING REMARKS

The problem of radio signal attenuation during hypervelocity reentry has been reviewed. It was shown that the signal loss was due to the presence of a high concentration of free electrons existing behind the bow shock of a reentering vehicle. The existence of electron concentration and signal loss was shown to be predictable and in qualitative agreement with actual flight results.

The results of experimental and theoretical work done on a forward facing jet were also reviewed. The existence of a region of large bow shock alteration by the jet was shown and this region was described in terms of jet-to-probe-diameter ratio, jet-to-free-stream pressure ratio, jet exit Mach number and angle of attack. Simplified theoretical considerations were given to the shock displacement phenomena which provided a possible explanation for the occurrence of the large shock displacements.

Finally application of the forward facing jet to the overall radio attenuation problem was considered. The advantages of the jet were stated and several simplified illustrations were given that showed that the jet could be used to help alleviate the blackout problem.

Although it has been stated that much more experimental and theoretical work in other phases of the overall problem need to be undertaken, the experimental results for the flow phenomena show that further work is worthwhile.

REFERENCES

1. Moeckel, W. E., and Weston, Kenneth C.: Composition of Thermodynamic Properties of Air in Chemical Equilibrium. NACA TN 4265, 1958.

2. Huber, Paul W., and Gooderum, Paul B.: Experiments With Plasmas Produced by Potassium Seeded Cyanogen Oxygen Flames for Study of Radio Transmission at Simulated Reentry Vehicle Plasma Conditions. NASA TN D-627, 1961.

3. Lin, S. C.: Rate of Ionization Behind Shock Waves in Air. Res. Rep. 170 (Contract No. AF 04(647) - 278), Avco-Everett Res. Lab., 1959.

4. Lin, S. C., and Teare, J. D., Shock Wave Structure in the Hypersonic Flight Regime. Presented at the A.P.S. Fluid Divisional Meeting at San Diego, California, November 24, 1958 Bull Am. Phys. Soc. II 4, (1959), p. 195.

5. Berman, M.: The Interaction of Electromagnetic Waves With the Plasma Surrounding a Reentry Vehicle. Air Force Technical Note BSD-TDR-62-57 SAE-TN-17-62, April 1962.

6. Lin, S. C.: A Rough Estimate of the Attenuation of Telemetering Signals Through the Ionized Gas Envelope Around a Typical Reentry Missile. Res. Rep. 74 (Contract No. AF 04(645) - 18), Avco-Everett Res. Lab., 1956.

7. Kuhns, Perry: Microwave Interferometer Measurements of Electron-Ion Recombination in Nitrogen, Air, and Argon. NASA TN D-1191, 1962.

8. NASA - University Conference on the Science and Technology of Space Exploration: Plasma Physics and Magnetohydrodynamics in Space Exploration. NASA SP-25. N63-11515.

9. Ellis, Macon C., Jr., and Huber, Paul W.: Radio Transmission Through the Plasma Sheath Around a Lifting Reentry Vehicle. NASA TN D-507, 1961.

10. Panofsky, Wolfgang K. H., and Phillips, Melba: Classical Electricity and Magnetism. Addison-Wesley Publishing Company, 1962.

11. Wilcox, Chas. H.: Effects of Atmospheric Attenuation on Reconaissance Antenna Design. Sci. Rep. No. 1 (AFCRD-TN-57-197, Contract AF 19(604) - 1708) Res. Lab., Hughes Aircraft Co., Feb. 20, 1927.

12. Lopatoff, Mitchel: Wing-Flow Study of Pressure-Drag Reduction at Transonic Speed by Projecting a Jet of Air From the Nose of a Prolate Spheroid of Fineness Ratio 6. NACA RM L51E09, Oct. 1951.

13. Love, Eugene S.: The Effects of a Small Jet of Air Exhausting From the Nose of a Body of Revolution in Supersonic Flow. NACA RM L52I19a, November 1952.

14. Hayman, Lovick O., and McDearmon, Russell W.: Jet Effects on Cylindrical Afterbodies Housing Sonic and Supersonic Nozzles Which Exhaust Against a Supersonic Stream at Angles of Attack From 90° to 180°. NASA TN D-1016, March 1962.

15. Charcyenko, Nickolai, and Hennessey, Katherine W.: Investigation of a Retrorocket Exhausting From the Nose of a Blunt Body Into a Supersonic Free Stream. NASA TN D-751, September 1961.

16. Peterson, Victor L., and McKenzie, Robert L.: Effects of Simulated Retrorockets on the Aerodynamic Characteristics of a Body of Revolution at Mach Numbers of From 0.25 to 1.90. NASA TN D-1300, May 1962.

17. Watts, G. A.: An Experimental Investigation of a Sonic Jet Directed Upstream Against a Uniform Supersonic Flow. Tech. Note No. 7, Inst. Aerophys., Univ. of Toronto, January 1956.

18. Romeo, David J., Sterrett, James R.: Exploratory Investigation of the Effect of a Forward-Facing Jet on the Bow Shock of a Blunt Body in a Mach Number 6 Free Stream. NASA TN D-1605, 1963.

19. Ferri, Antonio: Elements of Aerodynamics of Supersonic Flows. The Macmillan Co., 1949, pp. 169-178.

20. Love, Eugene S., Grigsly, Carl E., Lee, Louise P., and Woodling, Mildred J.: Experimental and Theoretical Studies of Axisymmetric Free Jets. NASA TR R-6, 1959.

21. Gooderum, Paul B., Wood, George P., and Breceroost, Maurice J.: Investigations With an Interferometer of the Turbulent Mixing of a Free Supersonic Jet. NACA TR 963, 1950.

22. Tollmien, Walter: Calculation of Turbulent Expansion Processes. NACA TM 1085, 1945.

23. Ames Research Staff: Equations, Tables, and Charts for Compressible Flow. NACA TR 1135.

24. Pope, Alan: Aerodynamics of Supersonic Flight. Pittman Publishing Corporation, 1950.

25. Sims, Theo E., and Jones, Robert F.: Rocket Exhaust Effects on
    Radio Frequency Propagation From a Scout Vehicle and Signal
    Recovery During the Injection of Decomposed Hydrogen Peroxide.
    NASA TM X-529, 1961.

VITA

<u>David Joseph Romeo</u>

Born in Syracuse, New York, June 19, 1936. Graduated from Syracuse University, Syracuse, New York in June 1958 from the College of Engineering, B.S.M.E. Employed briefly with Chance Vought Aircraft, Dallas, Texas, and presently employed by the National Aeronautics and Space Administration at Langley Station, Hampton, Virginia

37
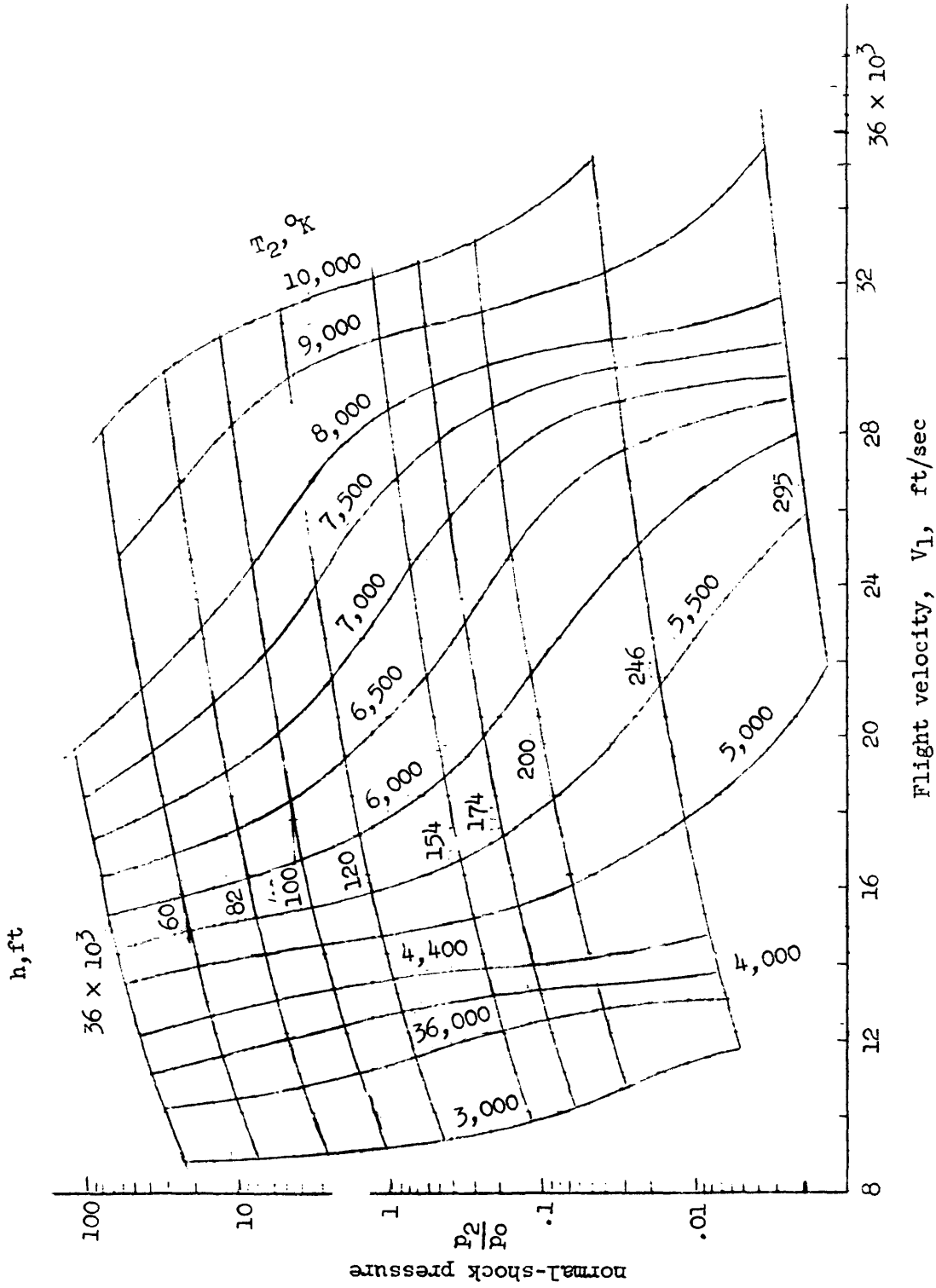
Figure 1.- Equilibrium hypersonic normal shock parameters in air.
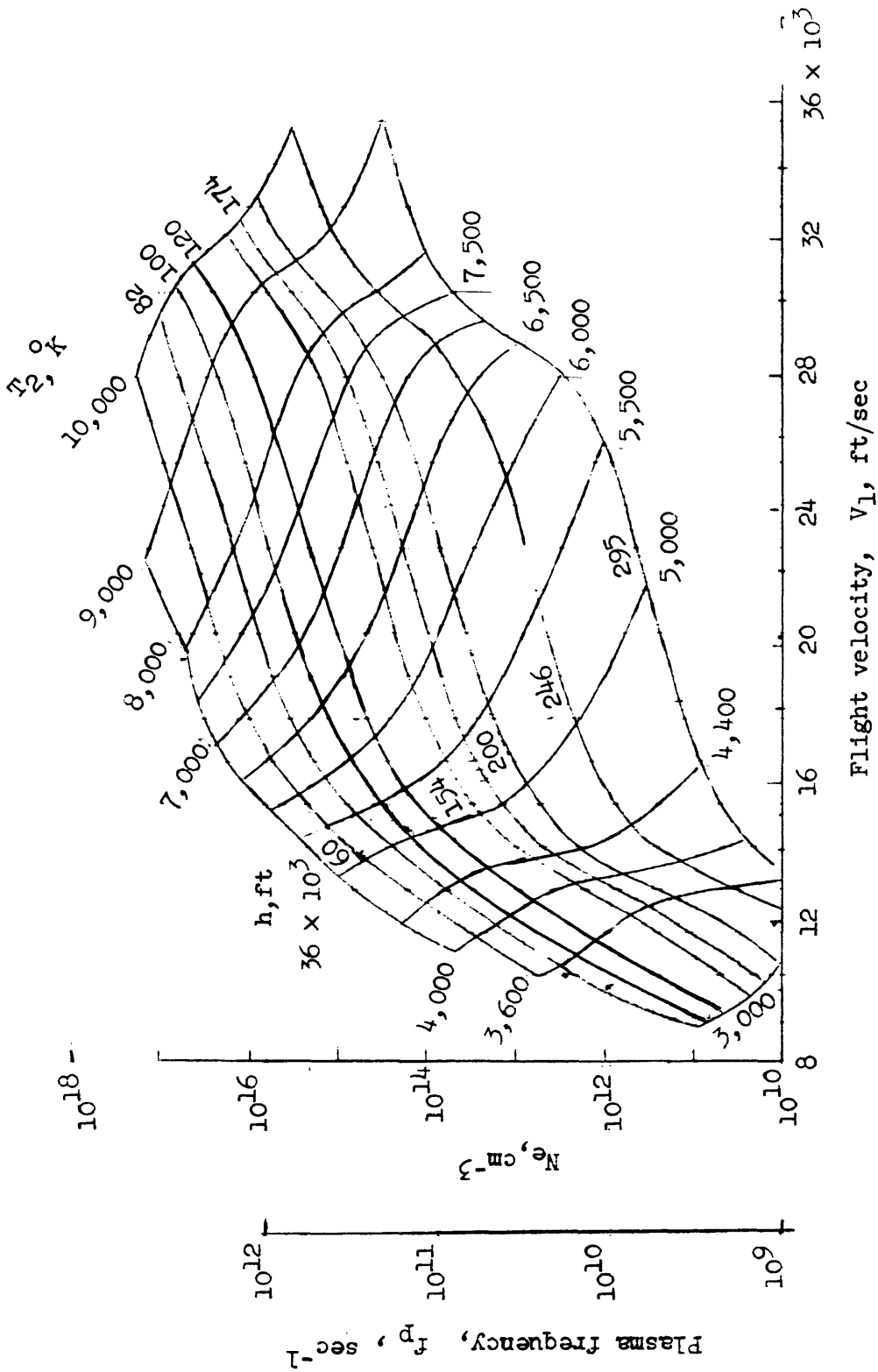
Figure 2.- Equilibrium electron concentration behind a normal shock in air.
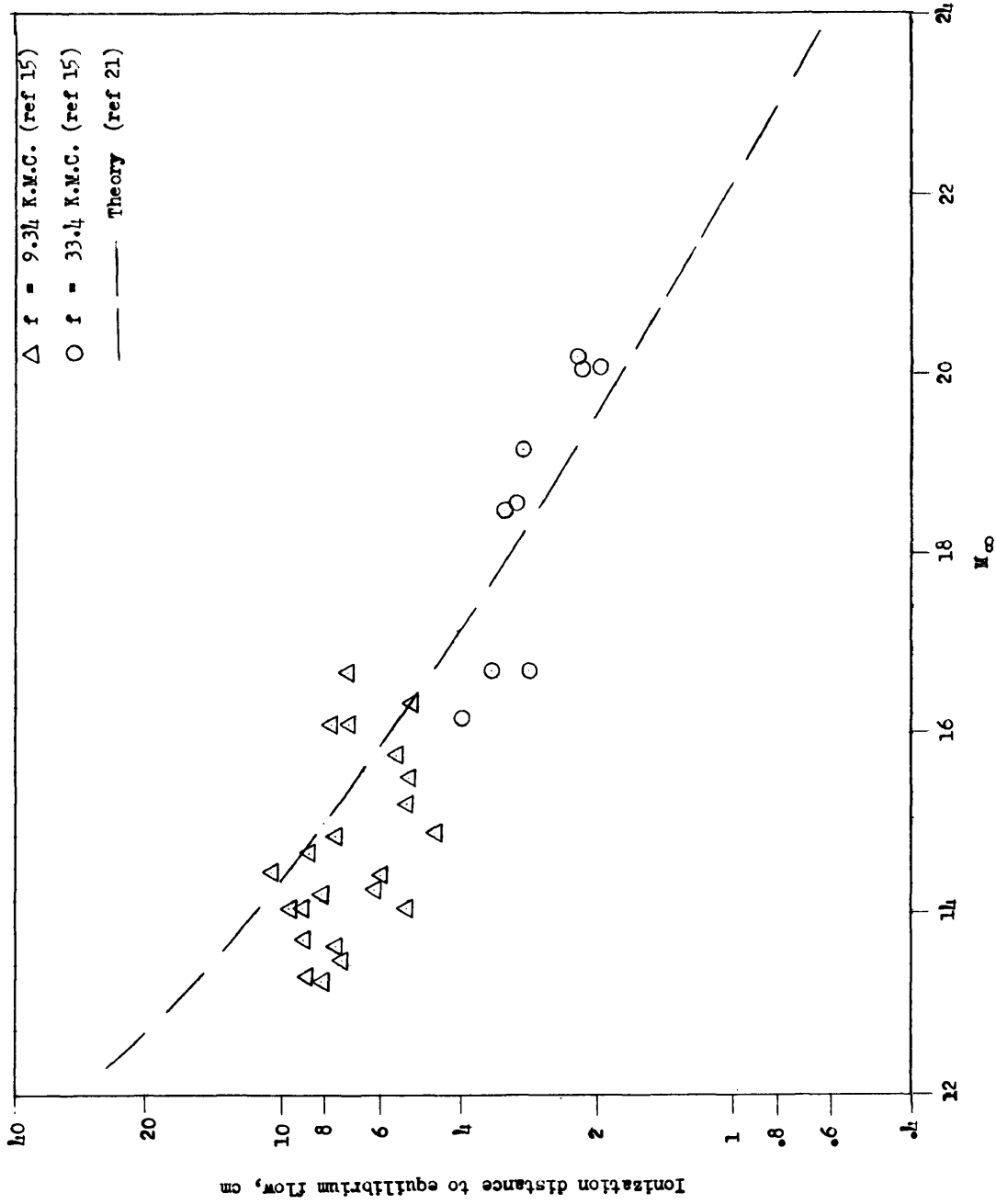
Figure 3.- Ionization distance behind normal shock for P_∞ = 20 microns (altitude of 250,000 ft; V = 15,000 ft/sec).

(a) $f_c \not\approx f_s$.
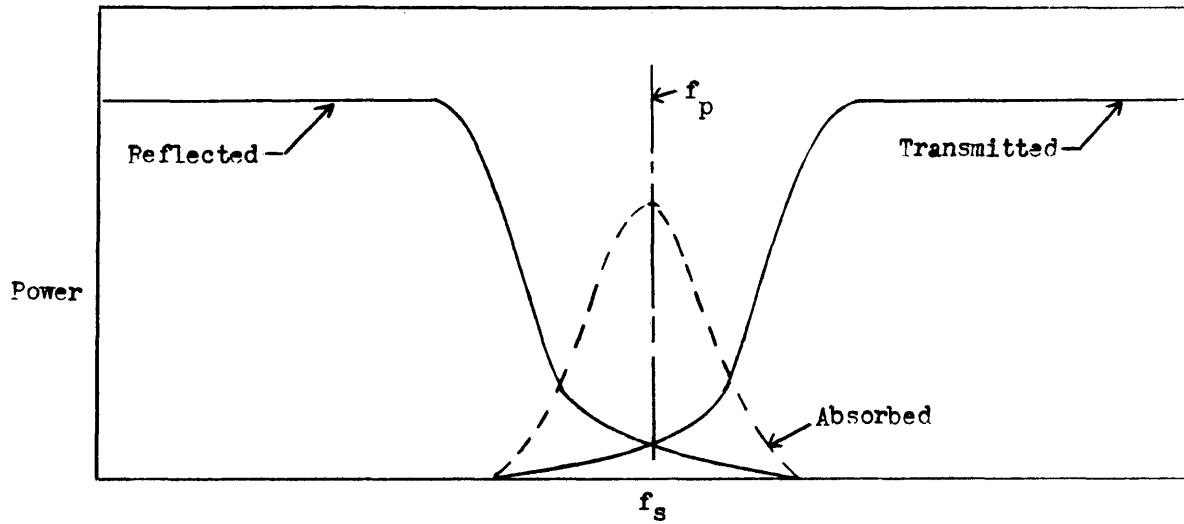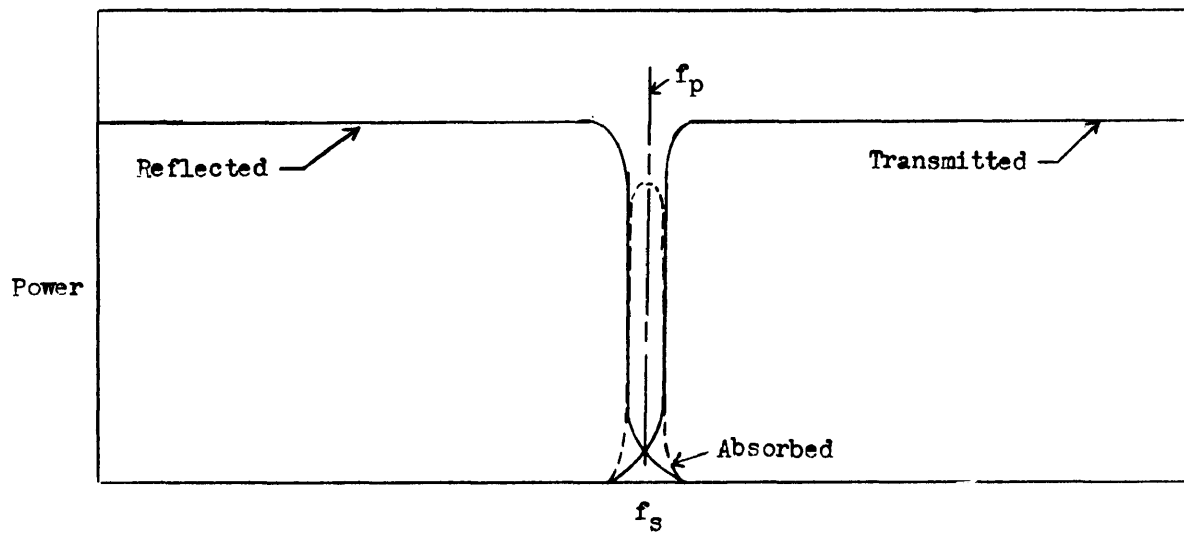
(b) $f_c \ll f_p$.

Figure 4.- Influence of collision frequency and plasma frequency on f_s reflection and absorption (attenuation).
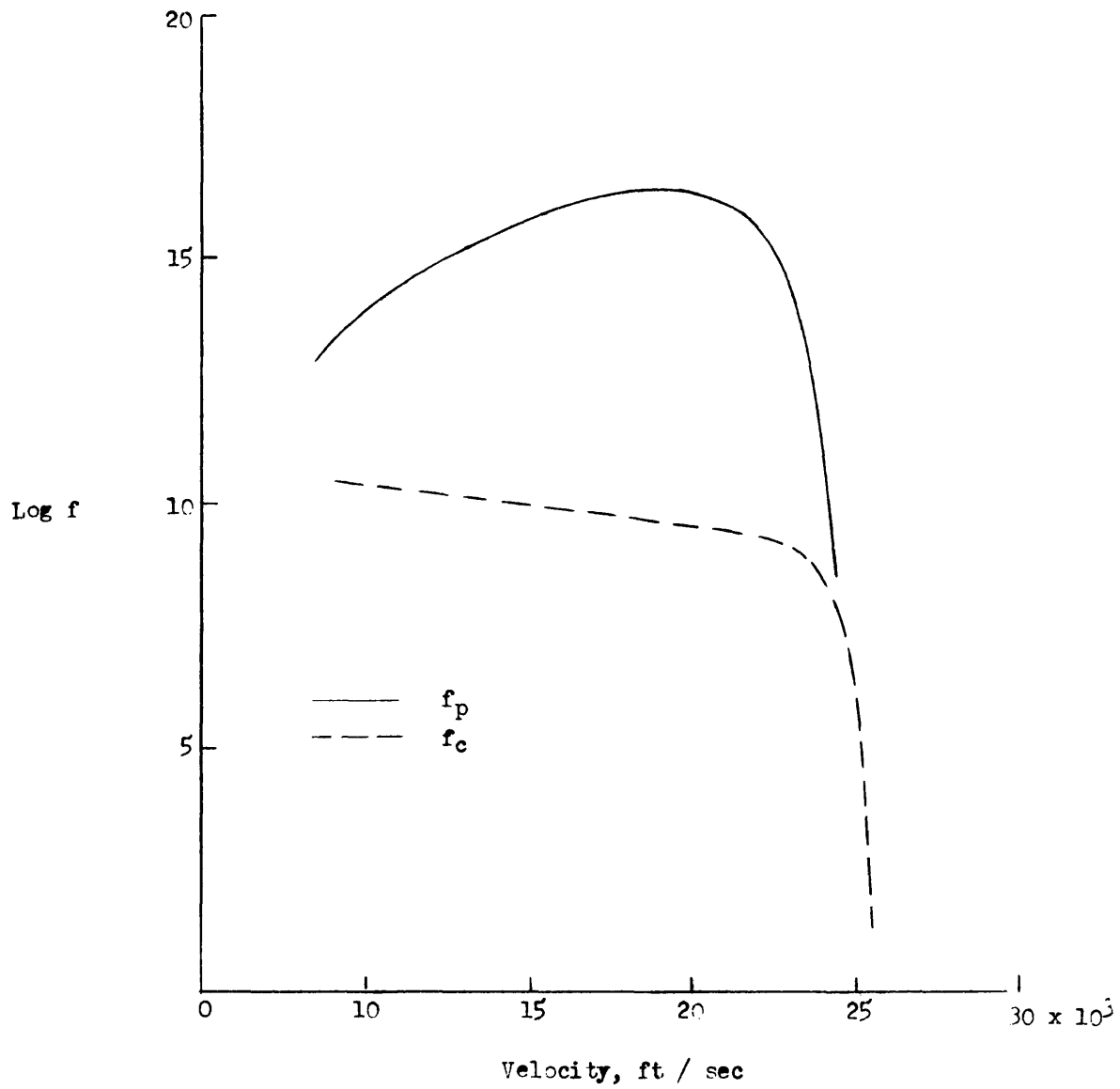
Figure 5.- Variation of plasma frequency and collision frequency
during reentry; typical trajectory.
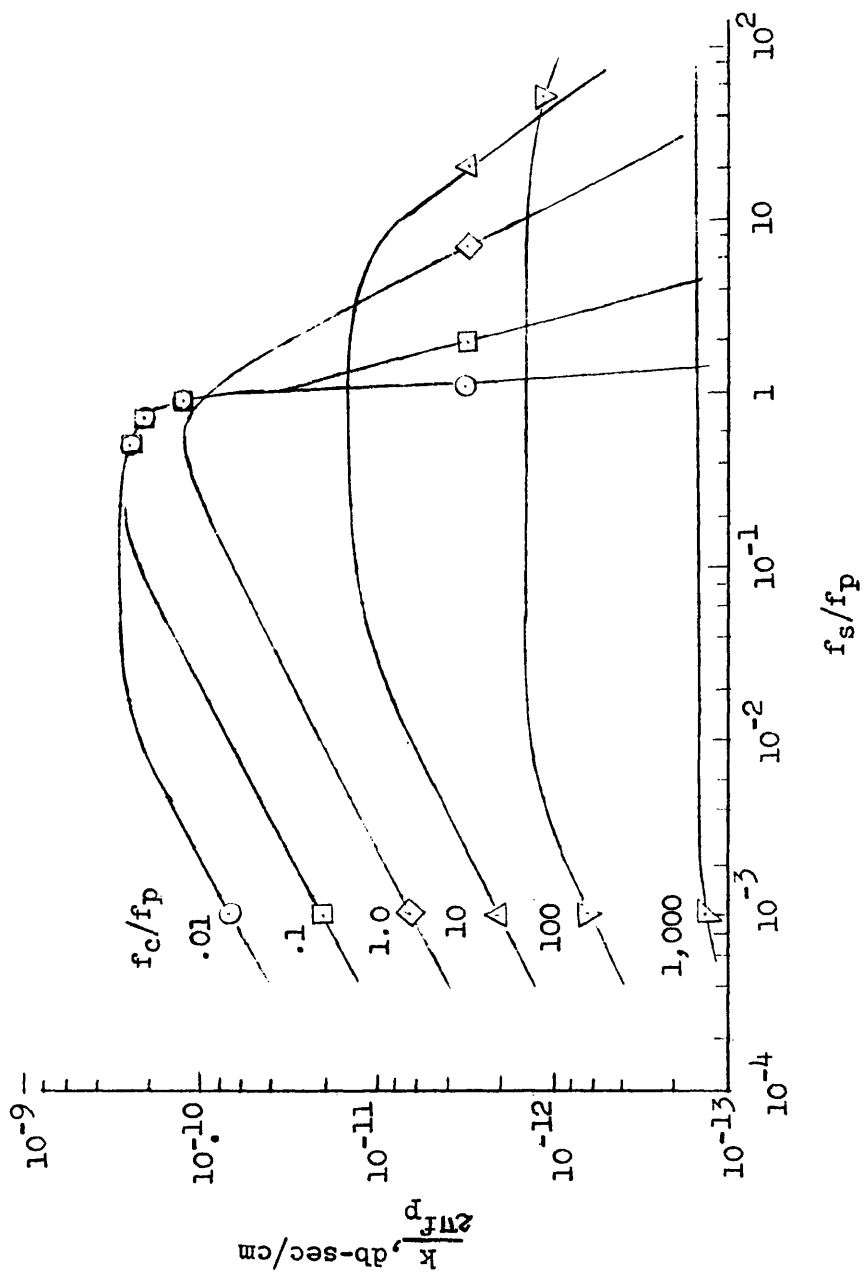
Figure 6.- Variation of signal attenuation with signal frequency for constant collision frequency.
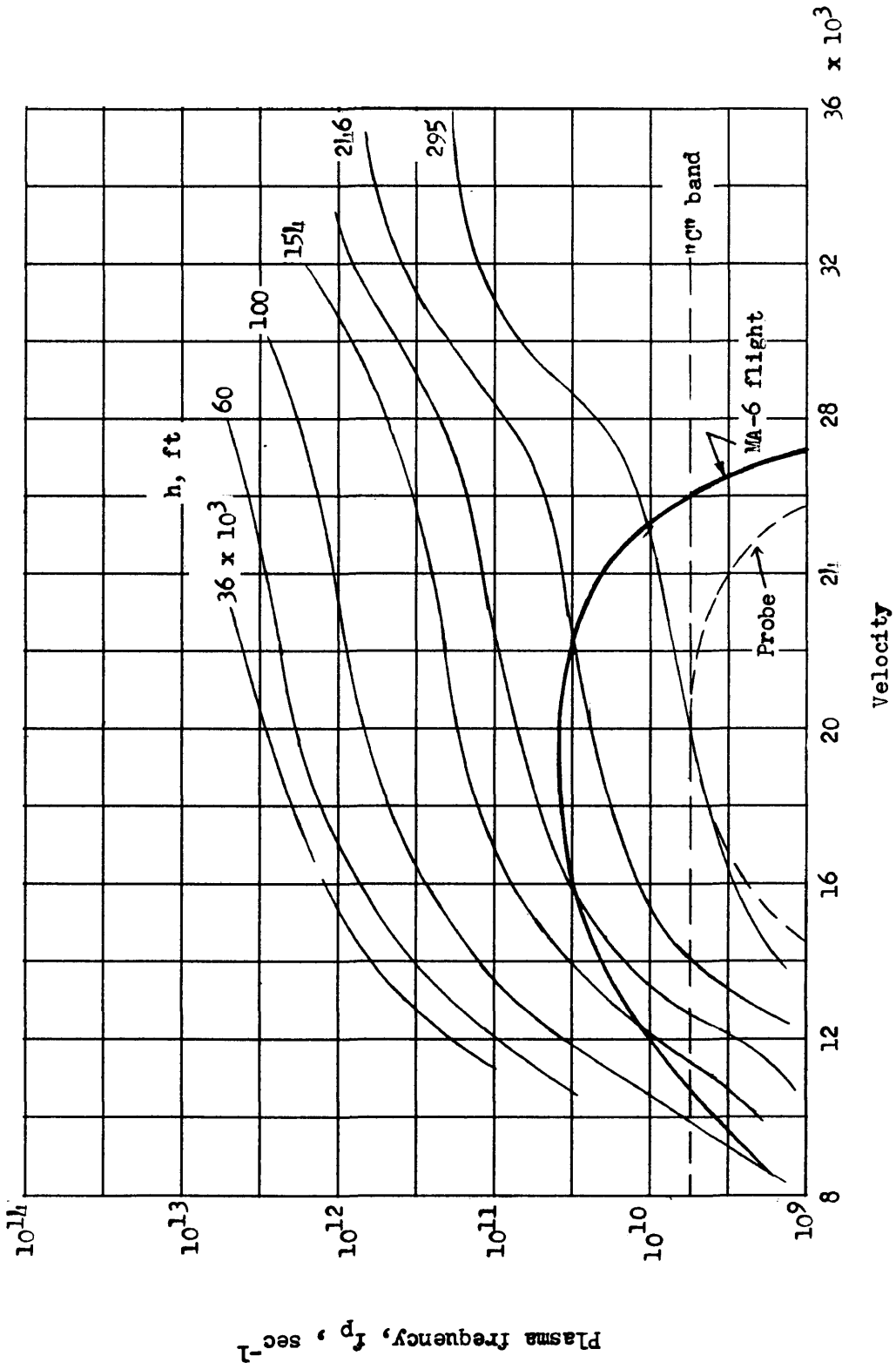
Figure 7.- Plasma frequency versus reentry velocity showing MA-6 trajectory and probe.
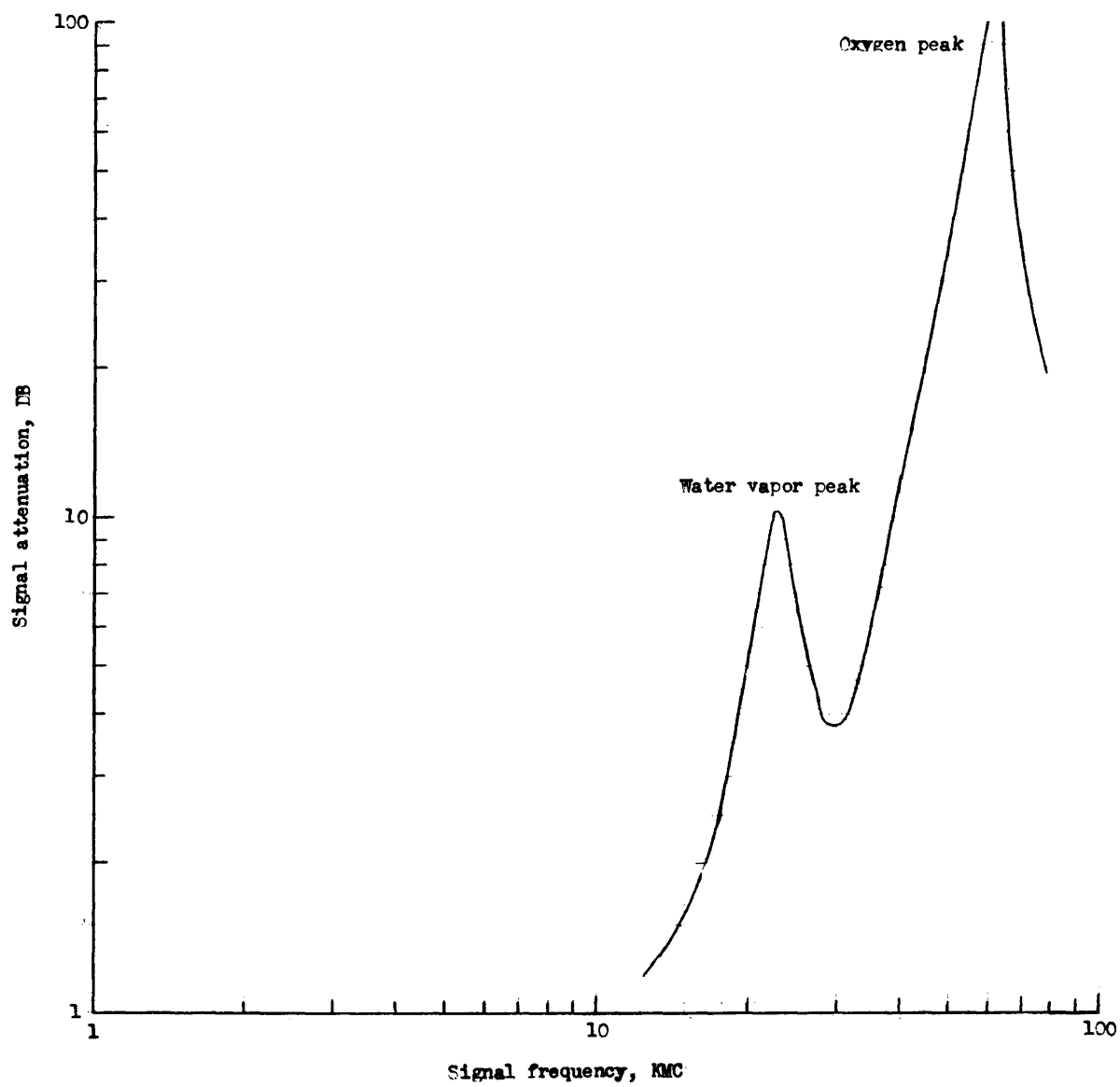
Figure 8.- Atmospheric attenuation showing upper limit on f_s.
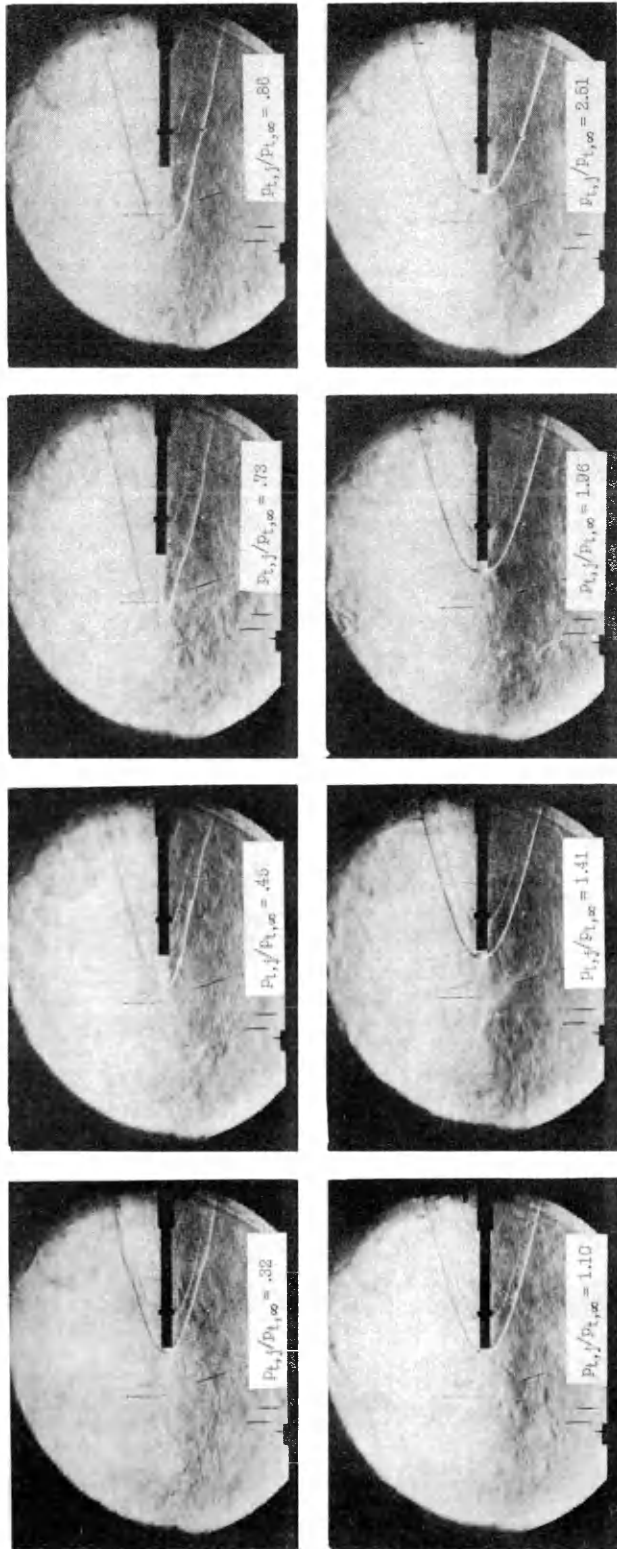
Figure 9.- Schlieren photographs of the effect of jet-to-free-stream total pressure ratio and model-to-jet-diameter ratio on main stream shock displacement distance for a nominal jet exit Mach number of 6.4; conical nozzle; $\alpha = 0^\circ$.
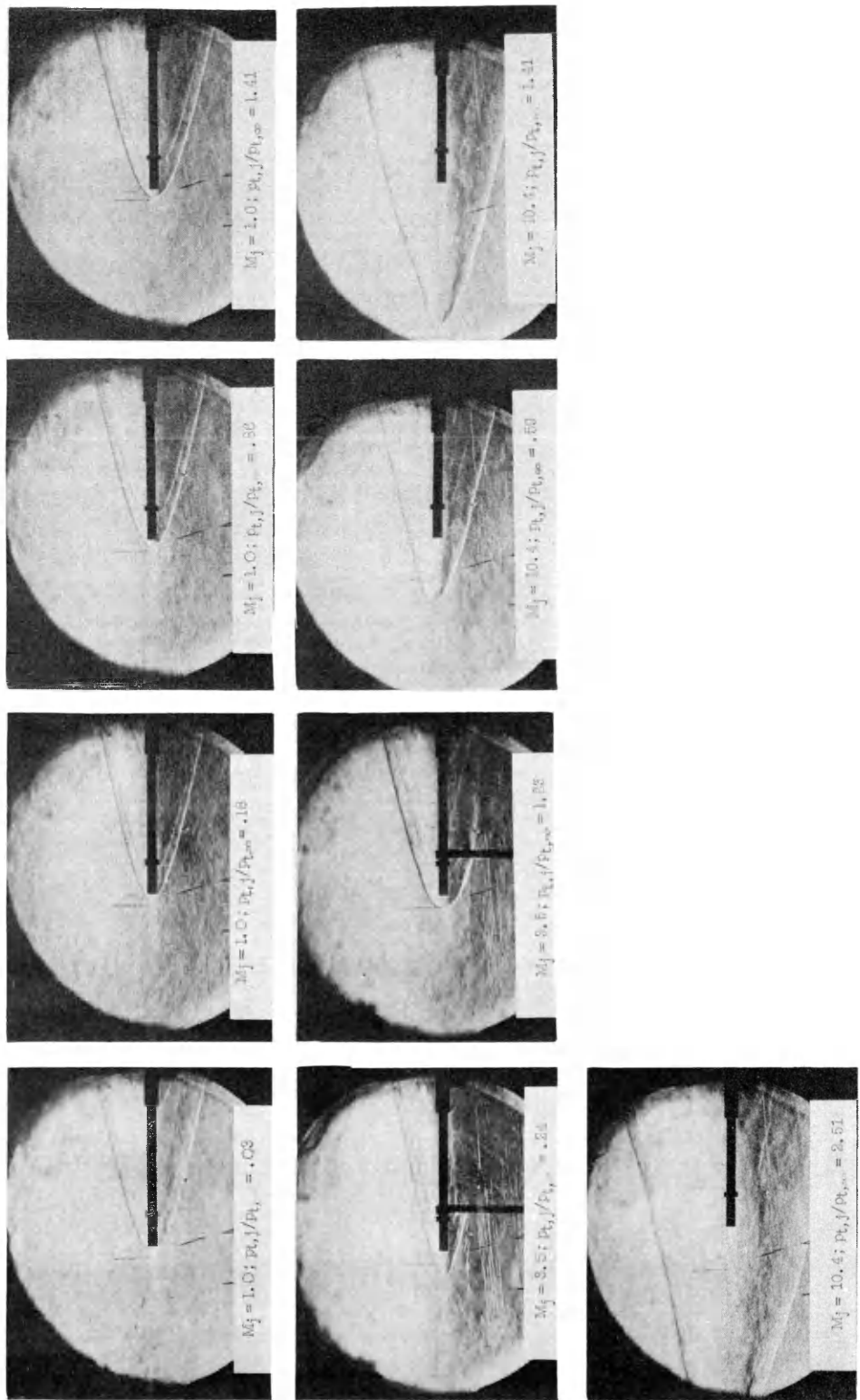
Figure 10.- Schlieren photographs of the effect of jet-to-free-stream total pressure ratio and main stream shock displacement distance for the tests (which were conducted) using helium; $\alpha = 0°$.

(a) Model 40; $d_m/d_j = 1.12$.

$p_{t,j}/p_{t,\infty}$
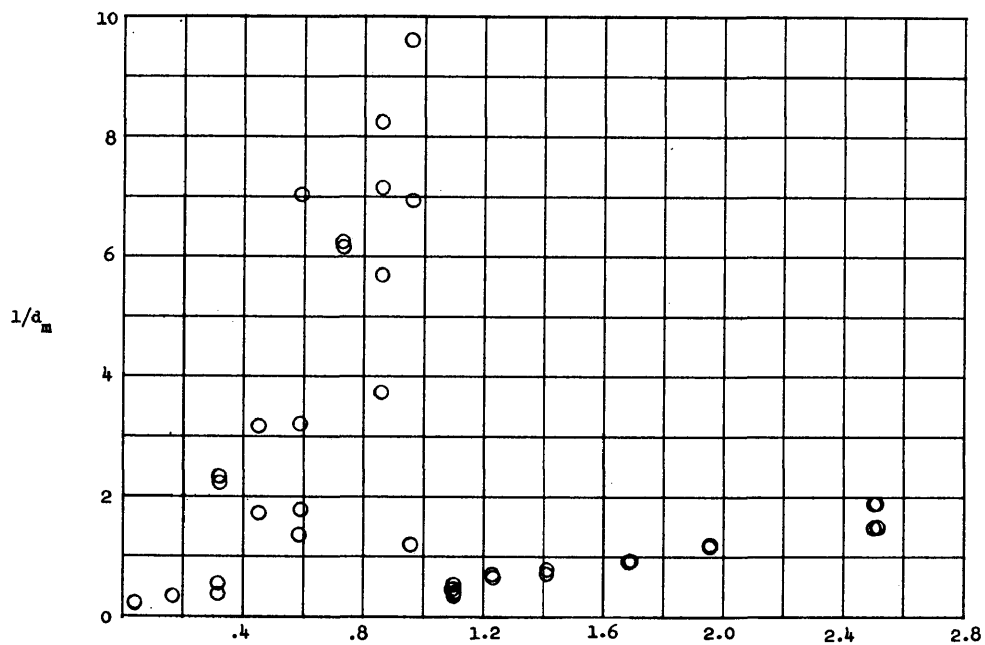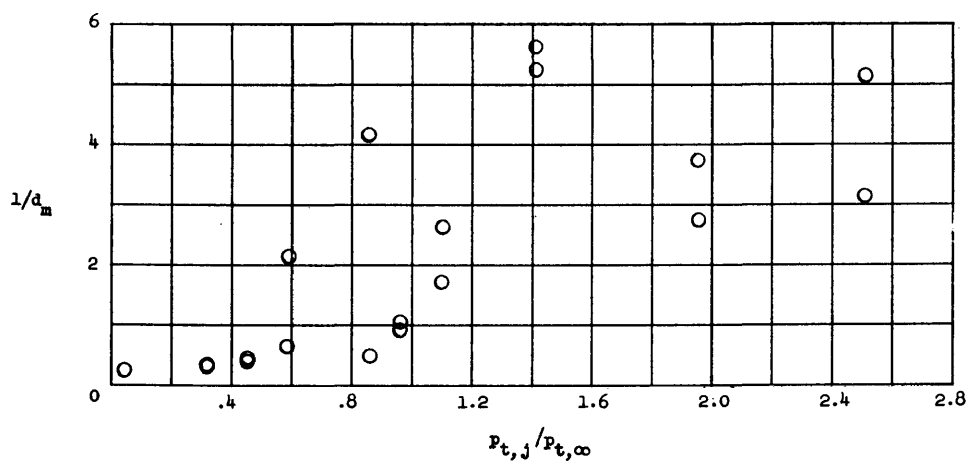
(b) Model 41; $d_m/d_j = 2.24$.

Figure 11.- Effect of jet-to-free-stream total pressure ratio on main stream shock displacement distance for a nominal jet exit Mach number of 6.4; conical nozzle; $\alpha = 0^\circ$.
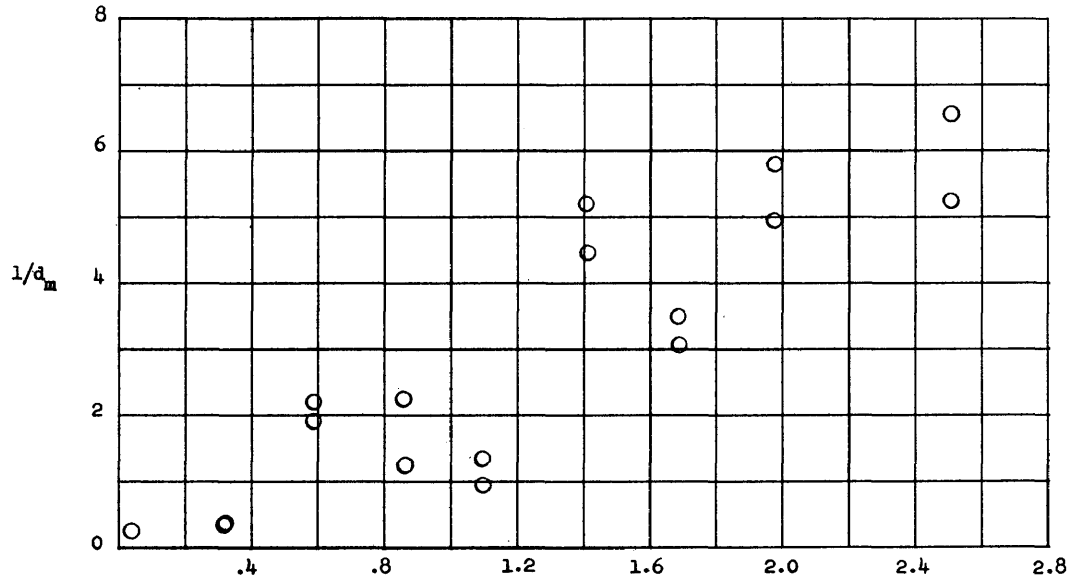
(c) Model 30; $d_m/d_j = 2.24$.

(d) Model 31; $d_m/d_j = 4.48$.

$p_{t,j}/p_{t,\infty}$
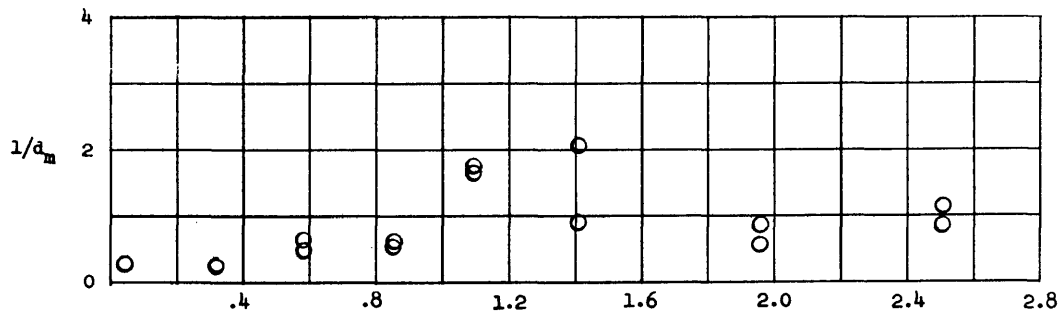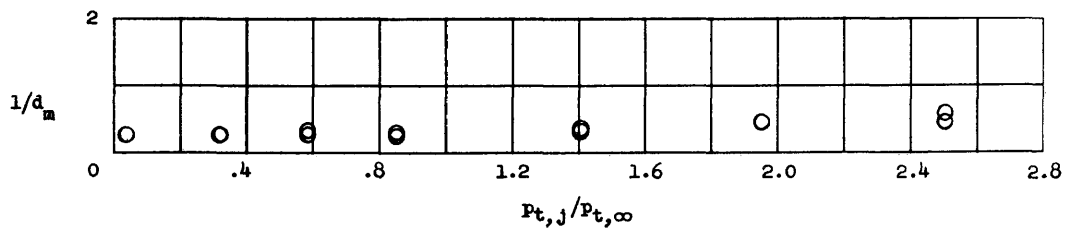
(e) Model 33; $d_m/d_j = 13.52$.

Figure 11.- Concluded.
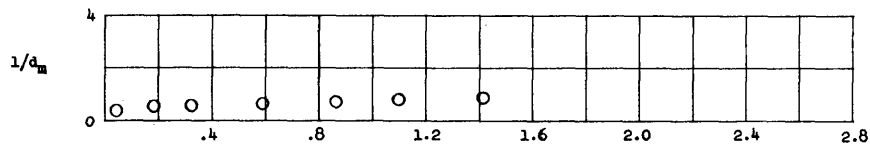
(a) Model 14; d_m/d_j = 9.62; M_j = 1.0.
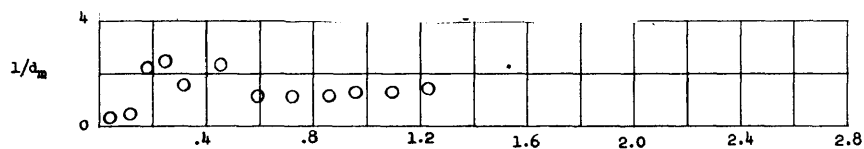
(b) Model 24; d_m/d_j = 4.68; M_j = 3.53.
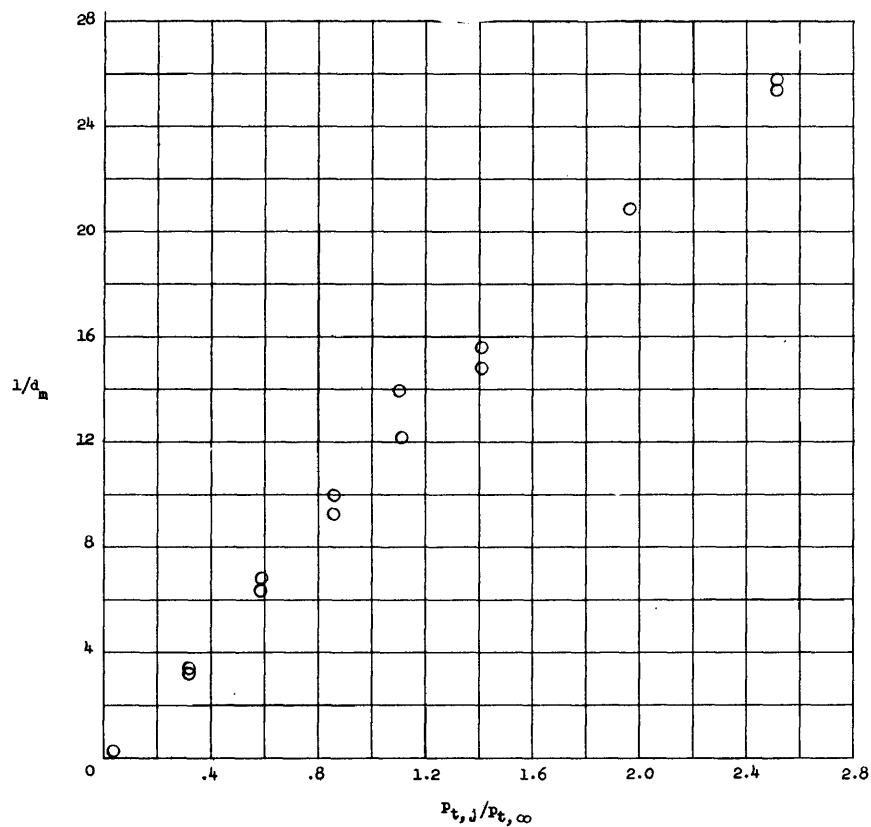
(c) Model 44; d_m/d_j = 1.12; M_j = 10.3.

Figure 12.- Effect of jet-to-free-stream total pressure ratio on main
   stream shock displacement distance for the tests which were conducted
   using helium; α = $0°$.
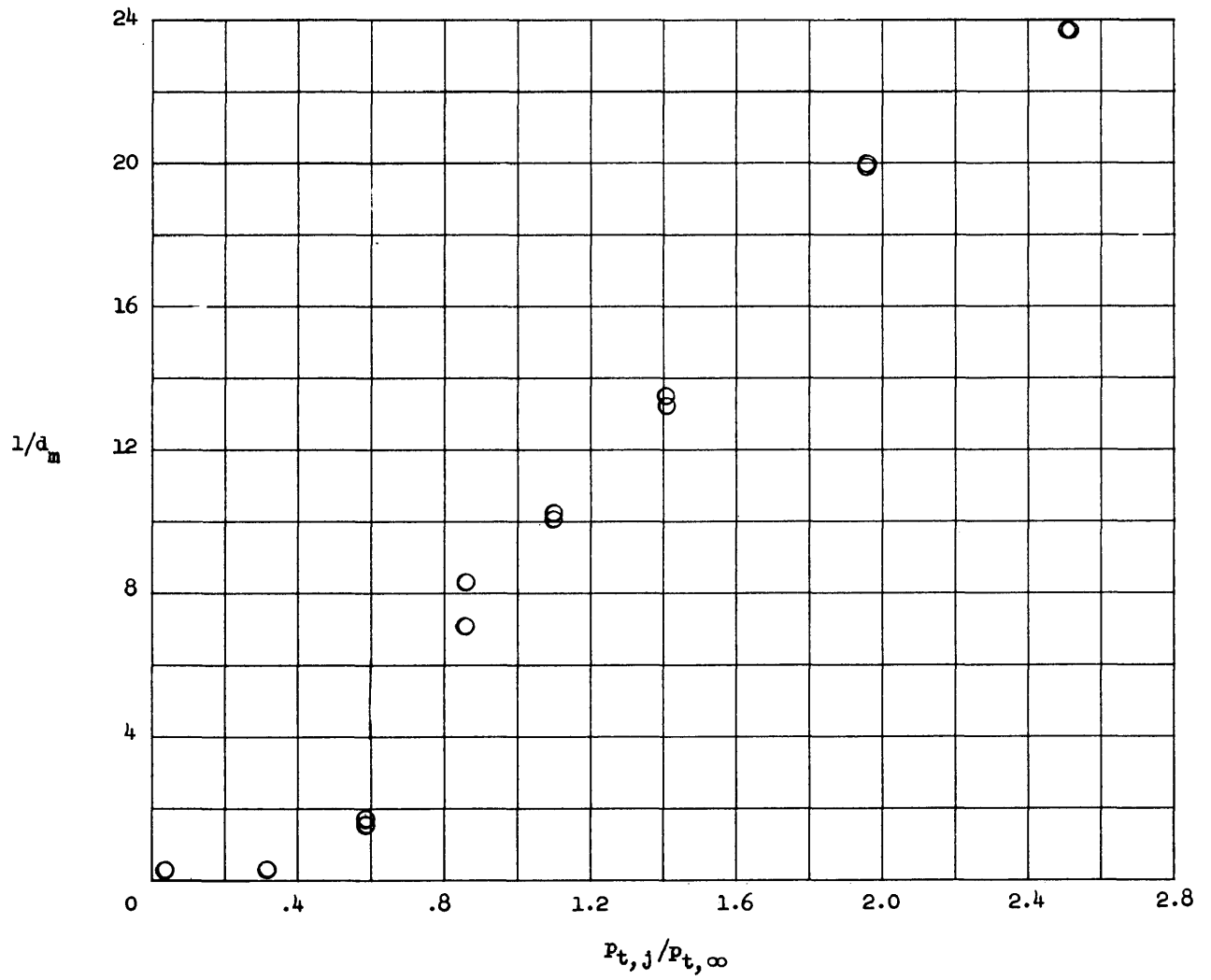
(d) Model 54; $d_m/d_j = 1.12$; $M_j = 10.3$.

Figure 12.- Concluded.

51
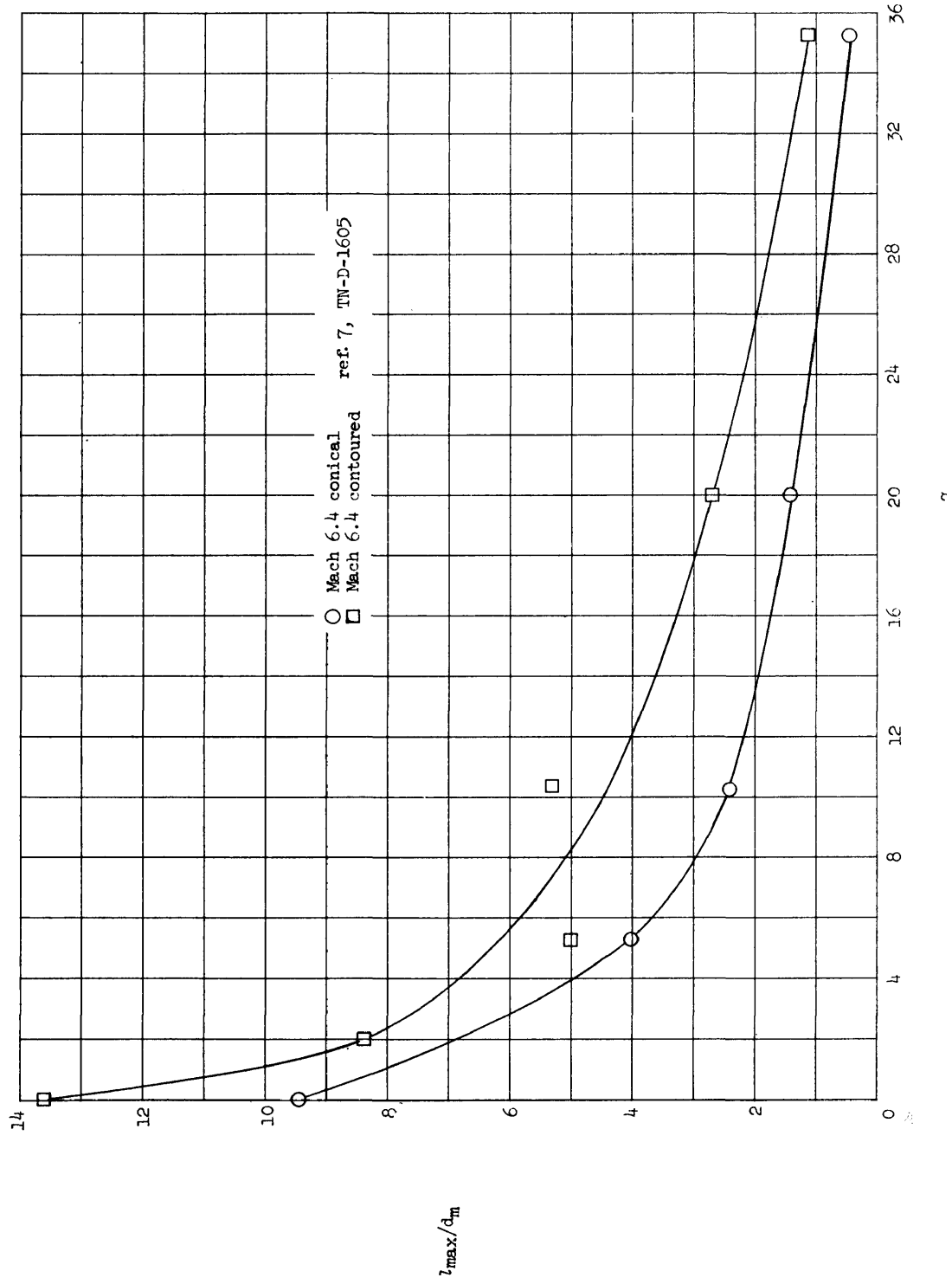
Figure 13.- Effect of angle of attack on maximum displacement for large displacement case.
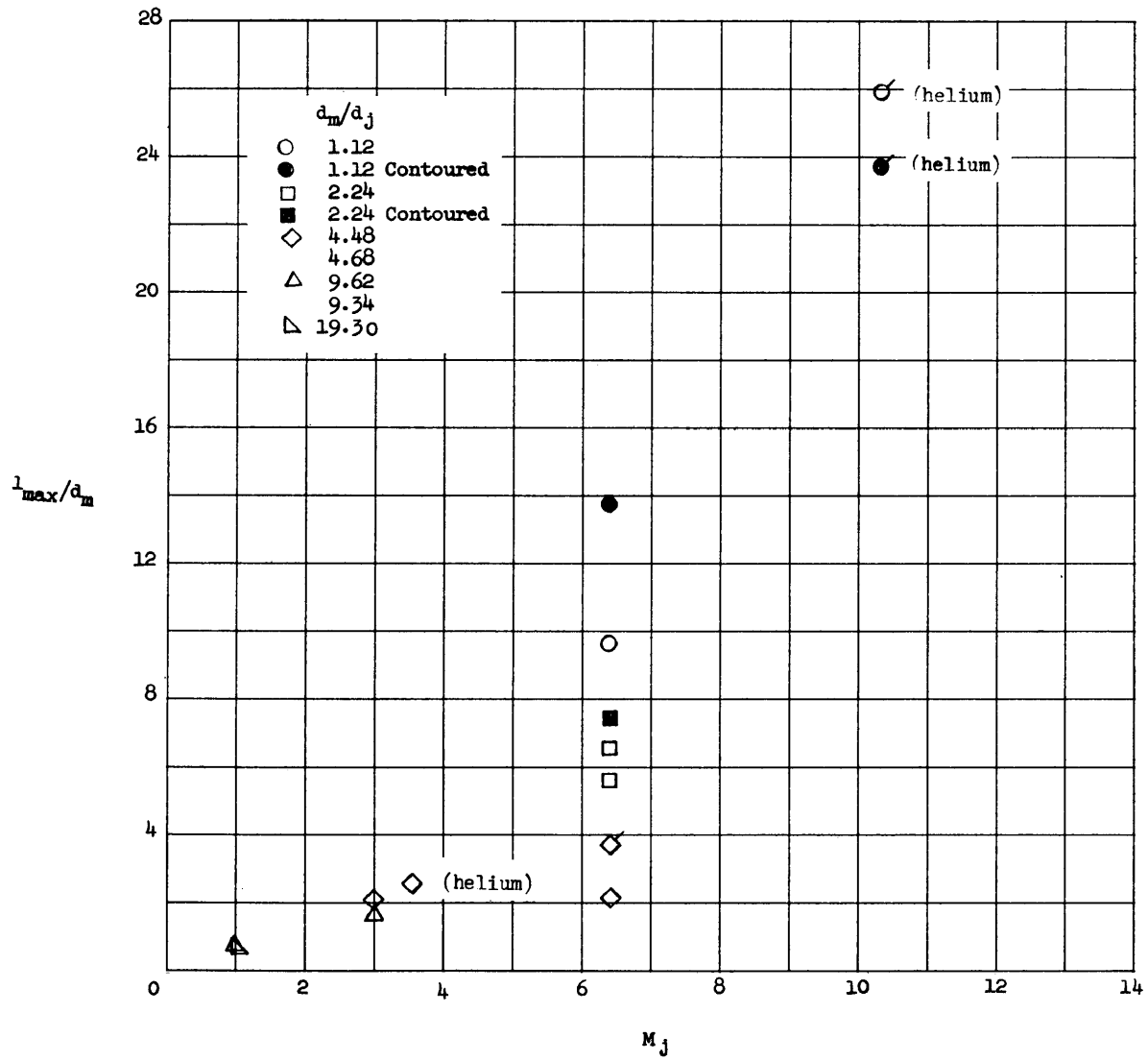
Figure 14.- Effect of jet exit Mach number on the maximum main stream shock displacement distance; $\alpha = 0°$. Flagged symbol indicates value may not have reached its maximum.
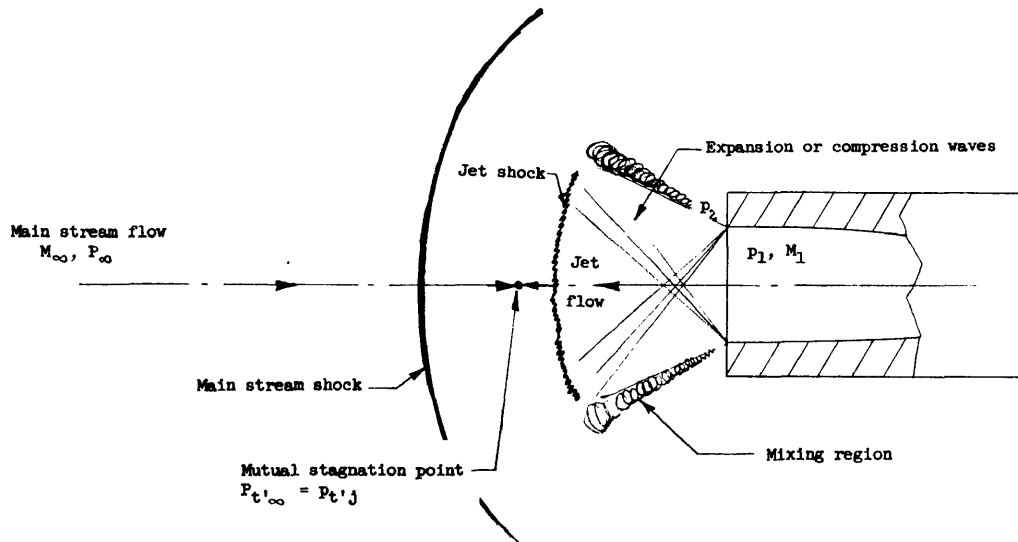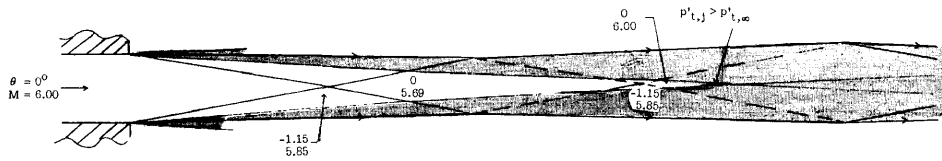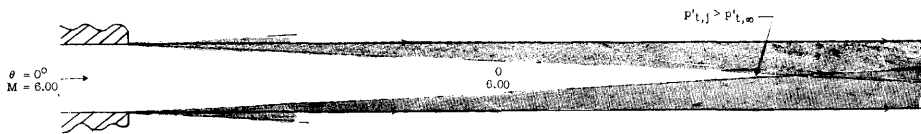
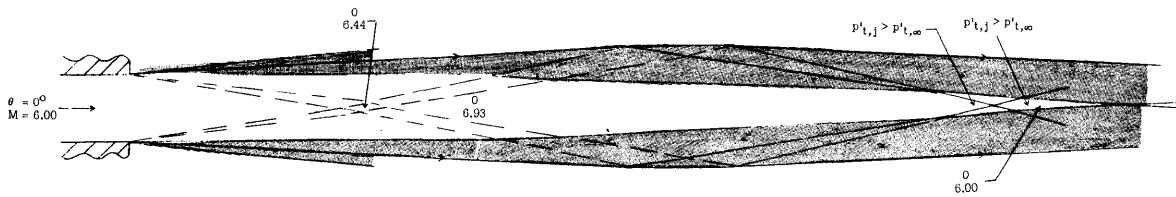(a).- Sketch of flow field for strong shock case.
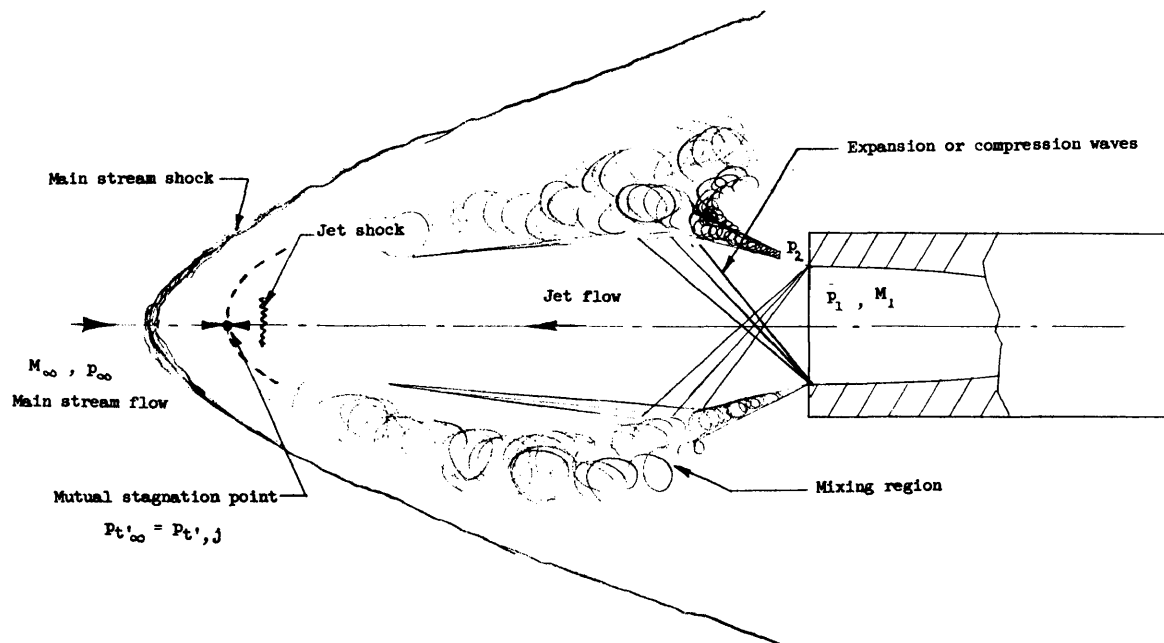
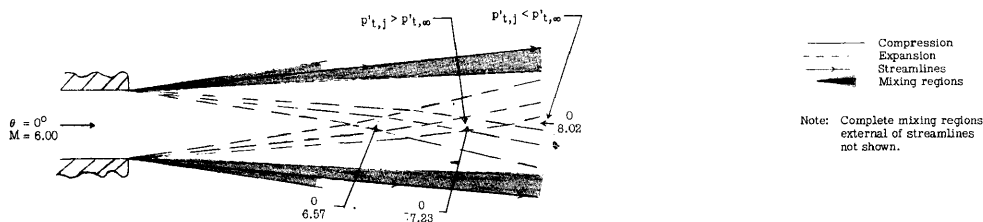Figure 15(b).- Sketch of flow field for large displacement case.

(a) Type of flow which corresponds to large displacement case (normal shock loss before mixing not sufficient for total pressure loss); $p_1/p_2 = 0.85$ and $p_{t,j}/p_{t,\infty} = 1.1$.

(b) Type of flow which corresponds to large displacement case (normal shock loss before mixing not sufficient for total pressure loss); $p_1/p_2 = 1.00$ when $p_{t,j}/p_{t,\infty} = 1.3$.

(c) Type of flow which corresponds to large displacement case (normal shocl loss before mixing not sufficient for total pressure loss); $p_1/p_2 = 1.54$ when $p_{t,j}/p_{t,\infty} = 2.00$.

(d) Type of flow which corresponds to strong shock case (normal shock loss before mixing sufficient for total pressure loss); $p_1/p_2 = 2.30$ when $p_{t,j}/p_{t,\infty} = 3.00$.

Figure 16.- Illustrations of two types of shock displacements, p_2/p_∞ assumed to be 1.30 for $M_\infty = 6.00$; $M_j = 6.00$.
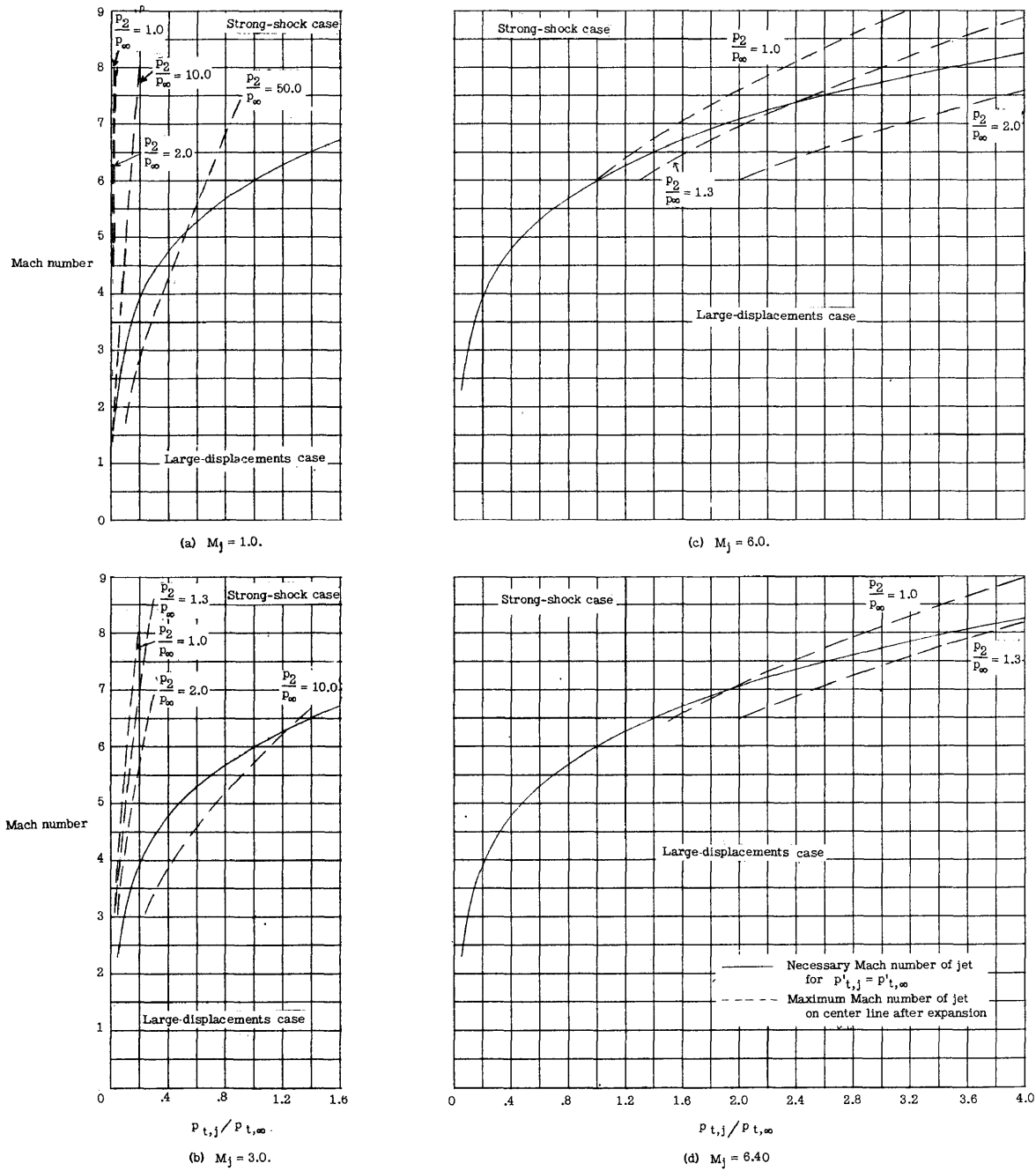
(a) $M_j = 1.0$

9

$\frac{p_2}{p_\infty} = 1.0$ Strong-shock case

$\frac{p_2}{p_\infty} = 10.0$ $\frac{p_2}{p_\infty} = 50.0$

$\frac{p_2}{p_\infty} = 2.0$

Mach number

Large-displacements case

(a) $M_j = 1.0$.

(c) $M_j = 6.0$

Strong-shock case $\frac{p_2}{p_\infty} = 1.0$

$\frac{p_2}{p_\infty} = 2.0$

$\frac{p_2}{p_\infty} = 1.3$

Large-displacements case

(c) $M_j = 6.0$.

(b) $M_j = 3.0$

9

$\frac{p_2}{p_\infty} = 1.3$ Strong-shock case

$\frac{p_2}{p_\infty} = 1.0$

$\frac{p_2}{p_\infty} = 2.0$ $\frac{p_2}{p_\infty} = 10.0$

Mach number

Large-displacements case

$p_{t,j}/p_{t,\infty}$

(b) $M_j = 3.0$.

(d) $M_j = 6.40$

Strong-shock case $\frac{p_2}{p_\infty} = 1.0$

$\frac{p_2}{p_\infty} = 1.3$

Large-displacements case

—— Necessary Mach number of jet for $p'_{t,j} = p'_{t,\infty}$

– – – – Maximum Mach number of jet on center line after expansion

0   .4   .8   1.2   1.6   2.0   2.4   2.8   3.2   3.6   4.0

$p_{t,j}/p_{t,\infty}$

(d) $M_j = 6.40$.

Figure 17.- Curves which illustrate possible regions for two types of shock displacements for different values of M_j; $\gamma = 1.40$, $M_\infty = 6.0$.
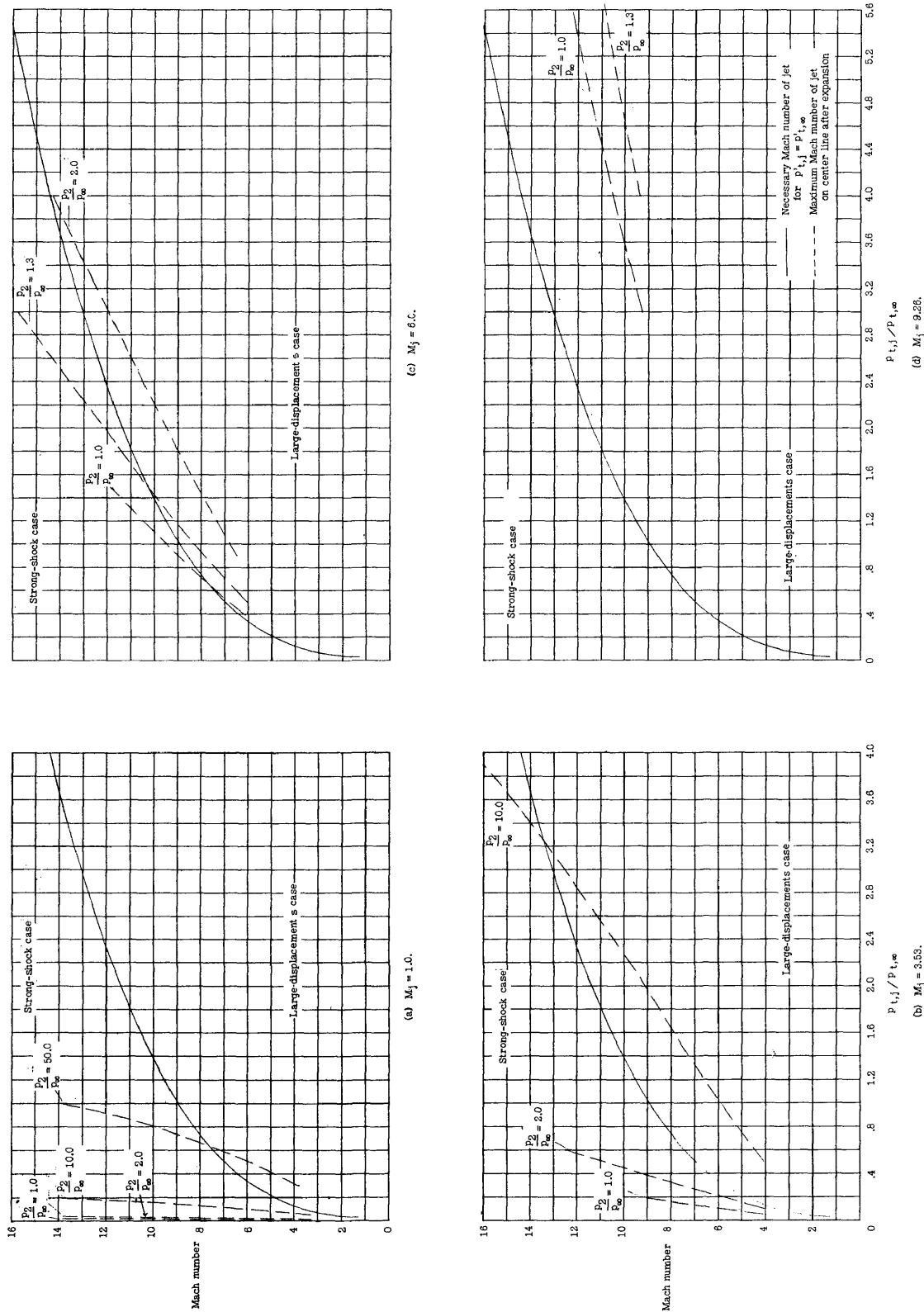
56

Figure 18.- Curves which illustrate possible regions for two types of shock displacements for different values of M_j; $\gamma = 1.666$ (helium) $M_\infty = 6.0$.
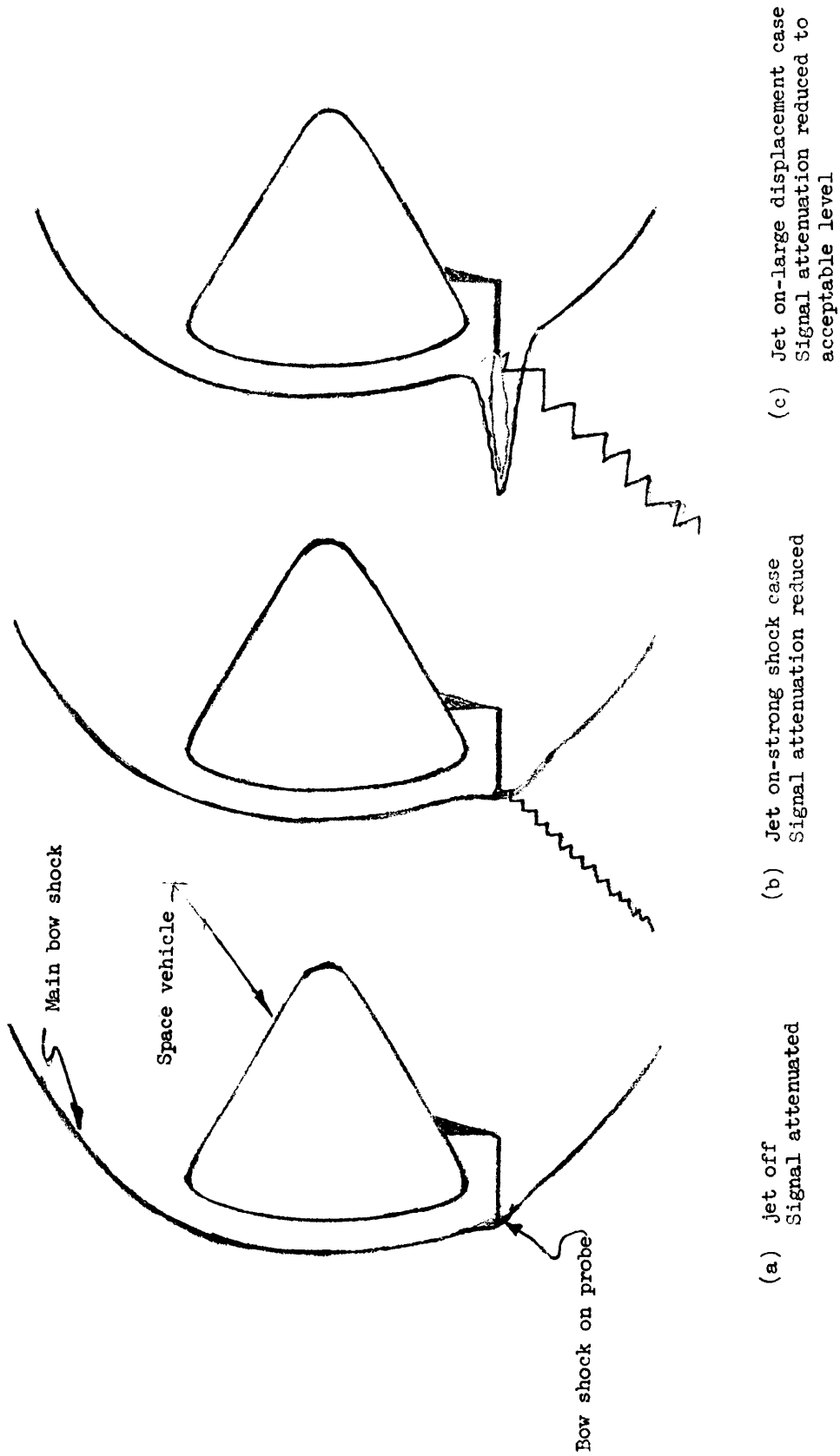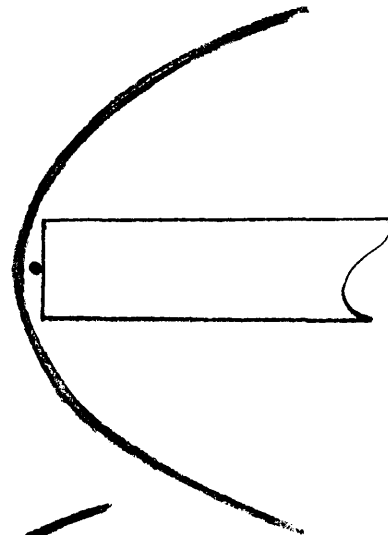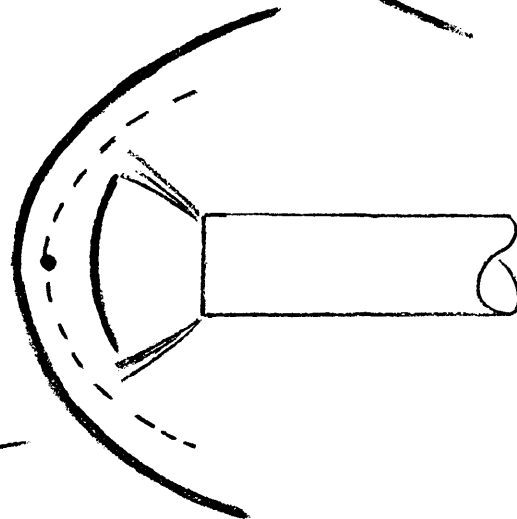
(a) Jet off
Signal attenuated

(b) Jet on-strong shock case
Signal attenuation reduced

(c) Jet on-large displacement case
Signal attenuation reduced to
acceptable level

Figure 19.- Sketch of antenna probe on space vehicle.

58

● ─ stagnation point

─ ─ ─ ─ ─ interface

(a) Jet off

(b) Jet on, strong shock case

(c) Jet on, large displacement case
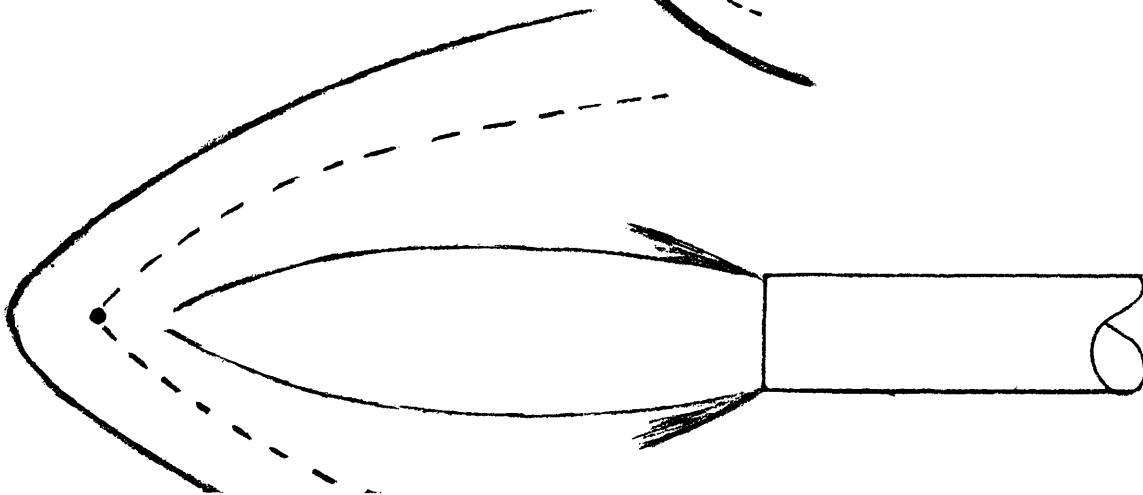
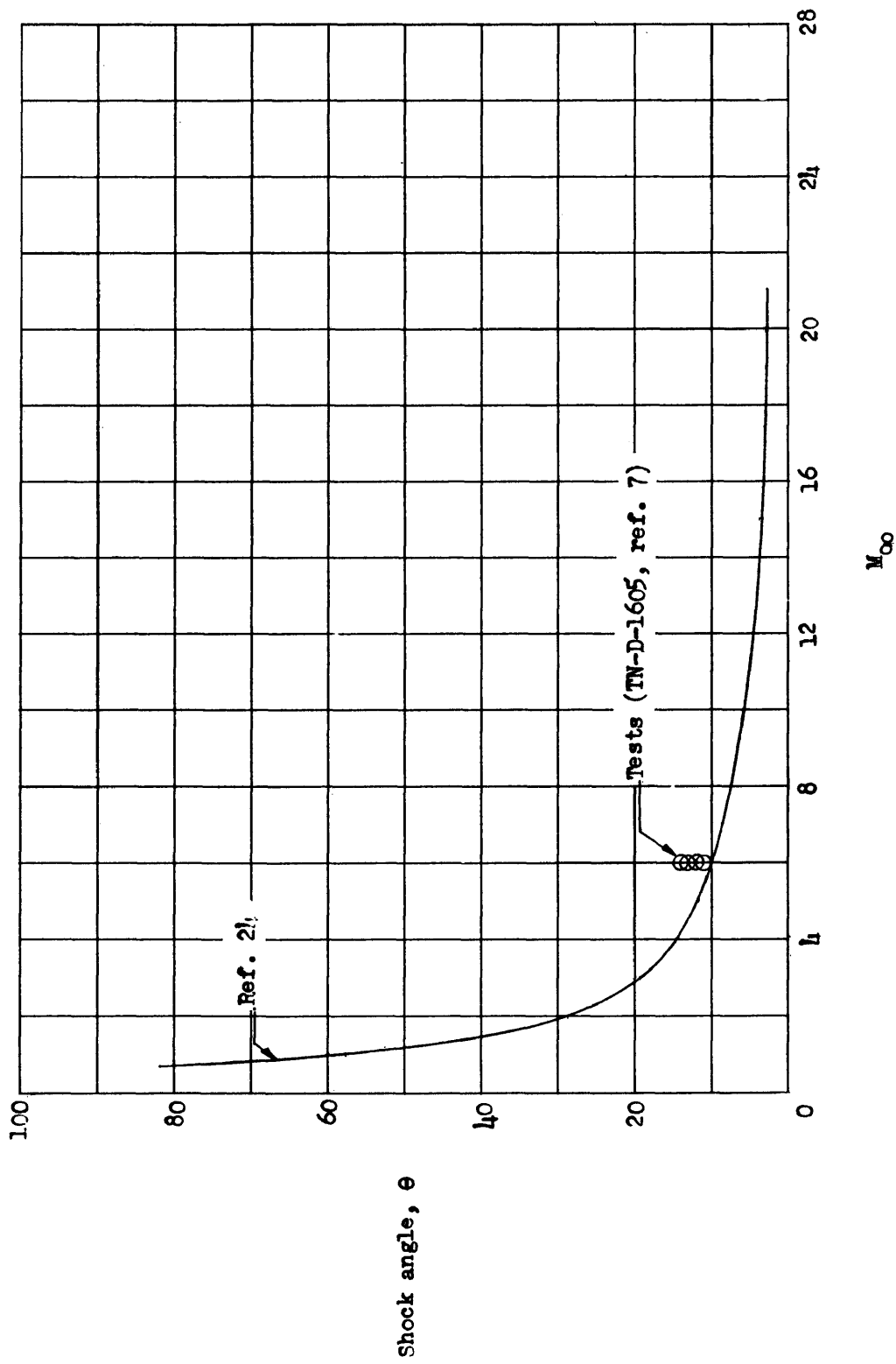Figure 20.- Sketch of antenna probe.

Figure 21.- Shock angle at probe versus free-stream Mach number, assuming θ equals Mach angle.
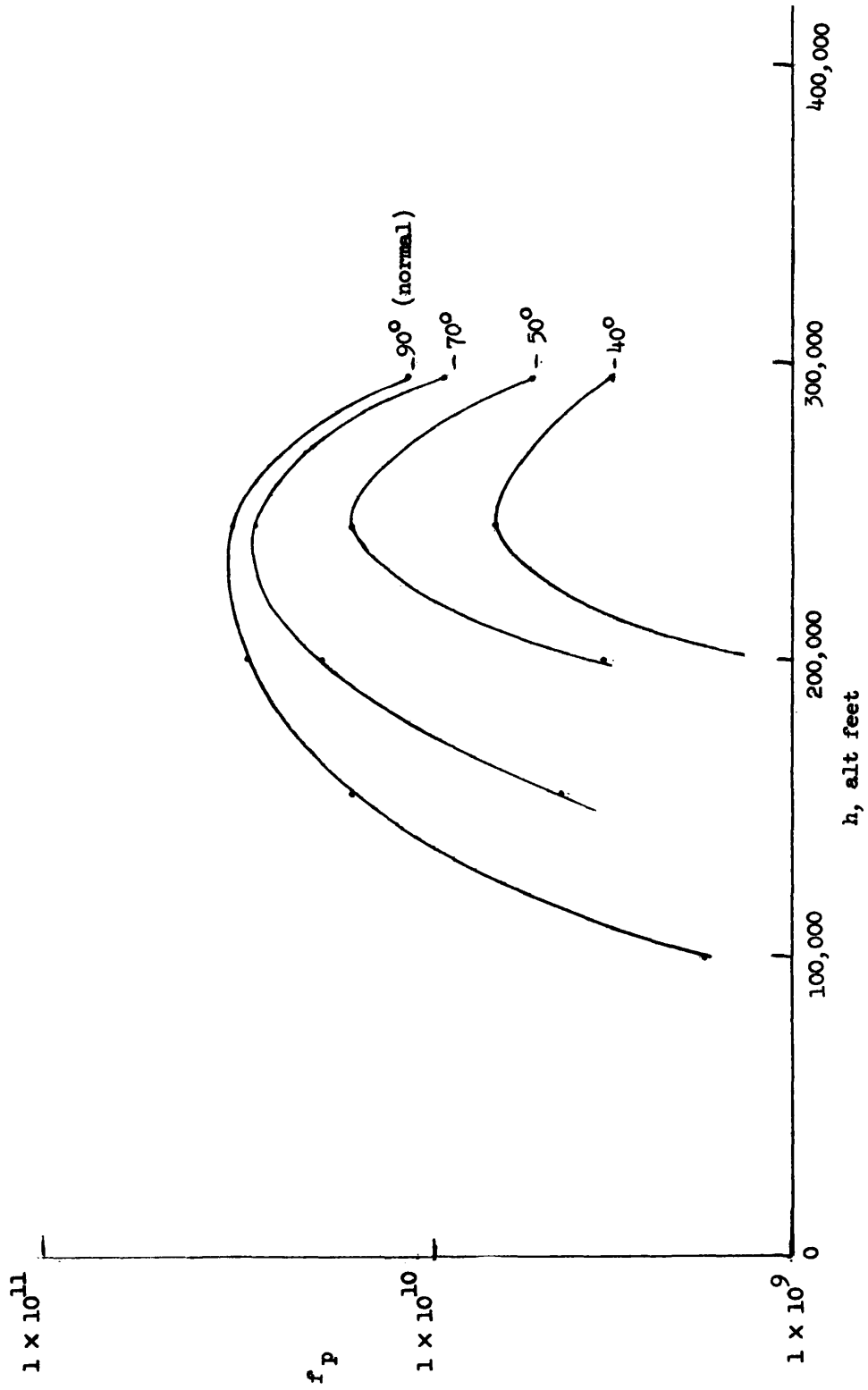
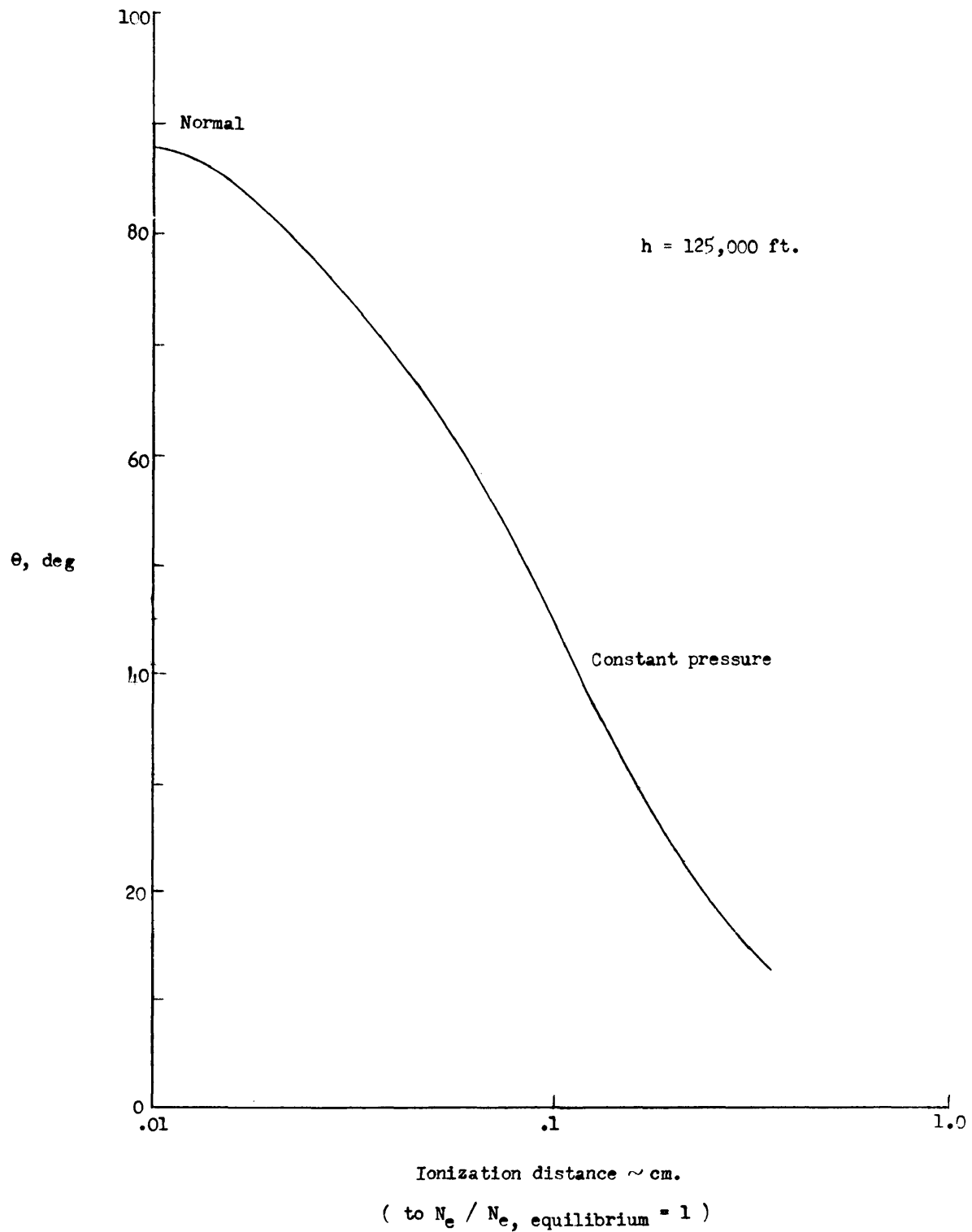Figure 22.- Plasma frequency versus altitude for various shock angles.

Figure 23.- Ionization distance to equilibrium as a function
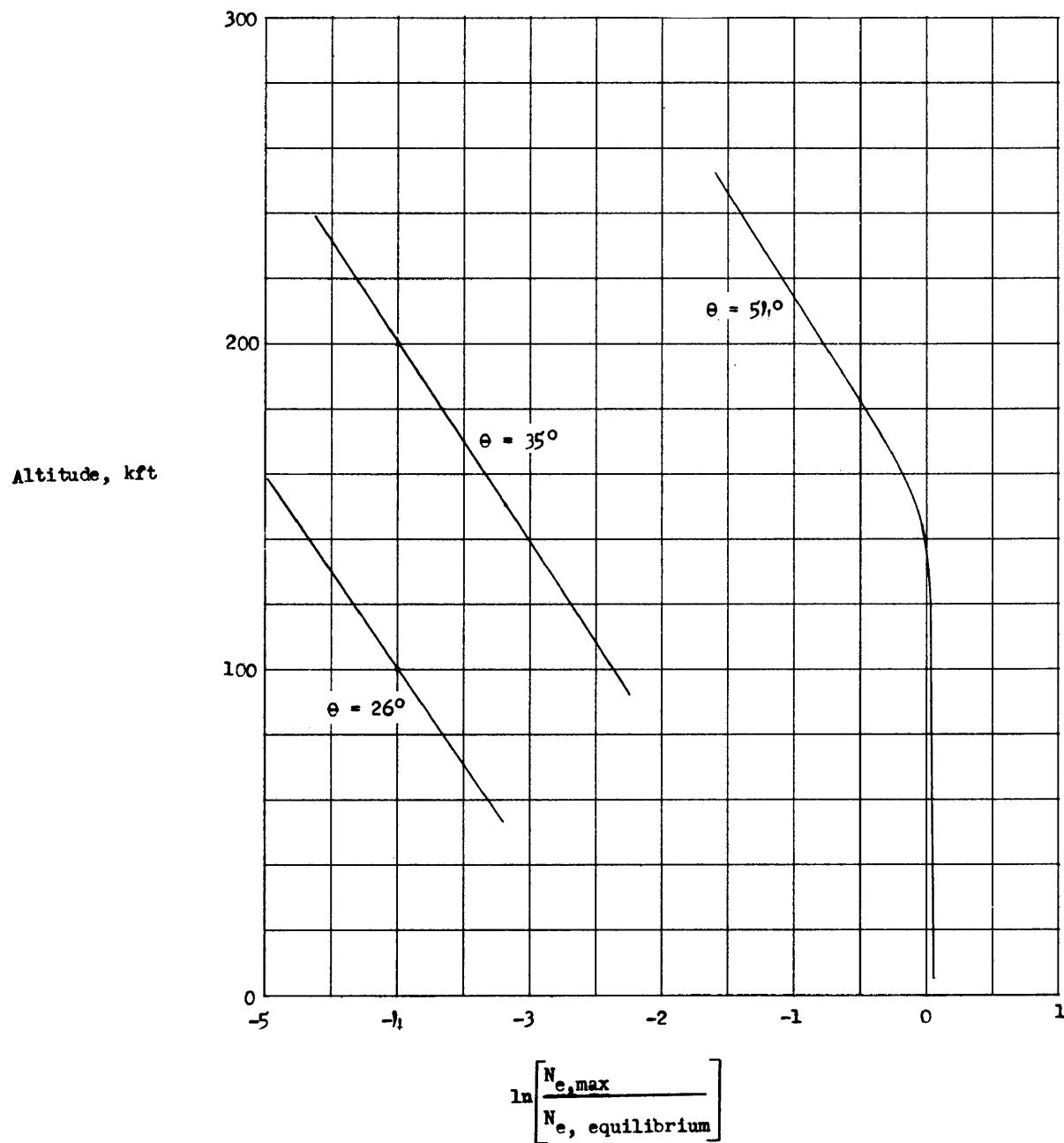of oblique shock angle.

Figure 24.- Nonequilibrium/equilibrium N_e versus altitude for various oblique shock angles; $V = 23,000$ fps.